energies

MDPI

Review

Research Progress and Perspectives of the Reaction Kinetics of Fe-Based Oxygen Carriers in Chemical Looping Combustion

Jiakun Mei [1], Shangkun Quan [1], Hairui Yang [2,3], Man Zhang [2,3], Tuo Zhou [2,3], Xi Yang [4], Mingyu Zhang [4], Tae-young Mun [5,6], Zhouhang Li [1], Ryang-Gyoon Kim [7], Xing Zhu [1], Hua Wang [1] and Dongfang Li [1,*]

[1] State Key Laboratory of Complex Nonferrous Metal Resources Clean Utilization, Faculty of Metallurgical and Energy Engineering, Kunming University of Science and Technology, Kunming 650031, China
[2] State Key Laboratory of Power Systems, Department of Energy and Power Engineering, Tsinghua University, Beijing 100084, China
[3] Key Laboratory for Thermal Science and Power Engineering of Ministry of Education, Department of Energy and Power Engineering, Tsinghua University, Beijing 100084, China
[4] Yunnan Energy Research Institute Co., Ltd., Kunming 650100, China
[5] Climate Change Research Division, Korea Institute of Energy Research (KIER), Daejeon 34129, Republic of Korea
[6] Graduate School of Energy Science and Technology, Chungnam National University, Daejeon 305764, Republic of Korea
[7] Research Institute of Industrial Science & Technology (RIST), Gwangyang 37673, Republic of Korea
* Correspondence: dongfang758520@gmail.com; Tel.: +86-17719987278

Abstract: Chemical looping combustion (CLC), a promising technology employing oxygen carriers to realize cyclic oxygen transfer between reactors, represents a transformative approach to CO_2 capture with near-zero energy penalties. Among oxygen carriers, Fe-based materials have emerged as the predominant choice due to their cost-effectiveness, environmental compatibility, and robust performance. The reaction kinetics of oxygen carriers are crucial for both material development and the rational design of CLC systems. This comprehensive review synthesizes experimental and theoretical advances in kinetic characterization of Fe-based oxygen carriers, encompassing both natural and synthetic materials, while different models corresponding to specific reaction stages and their intrinsic relationships with microstructural transformations are systematically investigated. The kinetic characteristics across various reactor types and experimental conditions are analyzed. The differences between fixed bed thermogravimetric analysis and fluidized bed analysis are revealed, emphasizing the notable impacts of attrition on the kinetic parameters in fluidized beds. Furthermore, the effects of temperature and gas concentration on kinetic parameters are profoundly examined. Additionally, the significant performance variation of oxygen carriers due to their interaction with ash is highlighted, and the necessity of a quantitative analysis on the competing effects of ash is emphasized, providing actionable guidelines for advancing CLC technology using kinetics-informed material design and operational parameter optimization.

Keywords: chemical looping combustion; Fe-based oxygen carrier; reaction kinetic; thermogravimetric analysis; fluidized bed reactors

check for updates

Academic Editor: Roberto García Fernández

Received: 31 March 2025
Revised: 23 April 2025
Accepted: 28 April 2025
Published: 30 April 2025

Citation: Mei, J.; Quan, S.; Yang, H.; Zhang, M.; Zhou, T.; Yang, X.; Zhang, M.; Mun, T.-y.; Li, Z.; Kim, R.-G.; et al. Research Progress and Perspectives of the Reaction Kinetics of Fe-Based Oxygen Carriers in Chemical Looping Combustion. *Energies* **2025**, *18*, 2313. https://doi.org/10.3390/en18092313

Copyright: © 2025 by the authors. Licensee MDPI, Basel, Switzerland. This article is an open access article distributed under the terms and conditions of the Creative Commons Attribution (CC BY) license (https://creativecommons.org/licenses/by/4.0/).

1. Introduction

Global warming has drawn significant attention worldwide. Studies have shown that the increase in the concentration of greenhouse gases in the atmosphere is the primary cause of the ongoing global warming [1]. Among them, CO_2 is the main greenhouse gas, accounting for more than 60% of the greenhouse effect [2].

Chemical looping combustion (CLC) technology has advantages such as near-zero energy consumption CO_2 capture [3–5]. The concept of CLC technology was first introduced by Richter et al. [6] in 1983. However, it was not until 1987 that Ishida et al. [7] formally named this new combustion method as CLC and proposed that CLC technology could be used to achieve CO_2 capture with extremely low energy consumption. The CLC system breaks down the process of the conventional fuel-air reaction into reduction and oxidation reactions, and the direct contact of the fuel with air is avoided by using an oxygen carrier to transfer the oxygen from the air into the fuel, achieving high-concentration CO_2 emissions in the flue gas for CO_2 capture [8,9]. Subsequently, Ishida et al. [7,10], for the first time, proposed the concept of combining a gas-turbine cycle to produce power with CLC while enabling CO_2 capture. The significant milestones in the development of CLC technology are summarized in Table 1.

Table 1. Significant milestones during the development of CLC technology.

Author/Organization	Year	Research Contents	Ref.
Lewis and Gilliland	1954	Reaction between metal oxides and carbonaceous fuels	[11]
Richter and Knoche	1983	Proposition of the concept of splitting the conventional combustion reaction into two cyclic redox reaction processes	[6]
Ishida and Jin	1994	Proposition of the concept of integrating CLC with a gas-turbine cycle for power generation while enabling CO_2 capture	[10,12]
Lyngfelt et al.	2001	Proposition of the concept of dual fluidized beds for CLC	[13]
Lyngfelt et al.	2004	10 kW_{th} gas fuel CLC test rig	[14]
Korea Institute of Energy Research	2005	50 kW_{th} gas fuel CLC test rig	[15]
Lyngfelt et al.	2008	Experiments on CLC of solid fuels	[16,17]
Shen et al.	2008		[18]
Alstom	2012	3 MW_{th} pilot-scale CLC units	[19]
Technical University of Darmstadt	2014	1 MW_{th} pilot-scale CLC units	[20]
Tsinghua University	2024	Auto-thermal continuous operation of a 5 MW_{th} CLC system	[21]

CLC systems are classified into two categories based on fuel type: gas fuel CLC and solid fuel CLC [22]. For gas fuel CLC, Lyngfelt et al. [13] introduced the concept of employing a dual fluidized bed for CLC and validated it using both cold and hot state tests, realizing chemical looping combustion with gaseous fuel. Lyngfelt [23] and colleagues at Chalmers University of Technology designed a 10 kW_{th} gas fuel CLC system. In this system, a fast fluidized bed served as the air reactor, and a bubbling fluidized bed served as the fuel reactor. With NiO used as the oxygen carrier, following a 100-h continuous operation, the system attained a fuel conversion rate exceeding 98%, and no CO_2 was detected at the outlet of the air reactor [14]. Korea Institute of Energy Research designed and constructed a 50 kW_{th} gas fuel CLC system, employing a circulating fluidized bed as the air reactor and a bubbling bed as the fuel reactor. Experimental results showed that the fuel conversion rate and CO_2 capture rate attained values as high as 99.7% and 98%, respectively [15]. The Spanish National Coal Institute devised and set up a 10 kW_{th} gas fuel CLC system with a

dual bubbling bed configuration and conducted evaluations of various oxygen carriers [24]. Bolhàr et al. [25] at the Vienna University of Technology constructed a 120 kW gas fuel CLC system with dual fast bed reactors. This system employed Ni-based oxygen carriers, demonstrating 98% CH_4 conversion and 94% CO_2 capture efficiency.

For solid fuel CLC, Lyngfelt et al. [26,27] explored the current state of the art, performance characteristics, and pilot scale experience of this process, and conclusions were drawn regarding oxygen carrier materials suitable for solid fuels, suggesting that the technology is ready for scale up. The research team led by Laihong Shen from Southeast University carried out CLC experiments using coal as the fuel, achieving a CO_2 capture efficiency of 80% at 960 °C with NiO as the oxygen carrier [28]. Thon et al. utilized a two-stage bubbling bed as the fuel reactor and a circulating fluidized bed riser as the air reactor, with lignite used as the solid fuel and ilmenite used as the oxygen carrier. They discovered that the two-stage fuel reactor performed well, and CO_2 concentrations in the dry off-gas exceeded 90 vol.% [29]. The investigations into solid fuel CLC systems are summarized in Table 2.

Table 2. The investigations into solid fuel CLC.

Author/Organization	Fuel	CLC System Scale	Ref.
Berguerand and Lyngfelt	Coal	10 kW_{th} CLC unit	[16]
Shen et al.	Biomass	10 kW_{th} reactor	[18]
Linderholm et al.	Bituminous coal and coke	10 kW_{th} CLC unit	[30]
Leion et al.	Petroleum coke, etc.		[31]
Bayham et al.	Sub-bituminous coal	25 kW_{th} CLC unit	[32,33]
University of Stuttgart University of Hamburg	Coal	10 kW_{th} CLC unit 25 kW_{th} CLC unit	[34]
Utah State University	Coal	200 kW_{th} CLC unit	[35]
Technical University of Darmstadt	Coal	1 MW_{th} CLC unit	[20]
Alstom	Coal	3MW_{th} CLC unit	[19]

Through the study of oxygen carriers, a critical component in CLC, Henrik Thunman et al. [36] introduced the concept of oxygen carrier-assisted combustion (OCAC) in 2013. They suggested that ilmenite's capacity to cyclically absorb and release oxygen could enhance oxygen distribution in circulating fluidized bed boilers. This approach replaces part or all of the bed material in solid fuel boilers with oxygen carriers to improve combustion efficiency. OCAC has been validated across fluidized bed boilers at laboratory, semi-industrial, and full-industrial scales [36–41].

Oxygen carriers are undoubtedly critical components in CLC technology [42]. Fe-based oxygen carriers exhibit significantly lower costs than other transition metal-based oxygen carriers due to their abundant reserves as well as mature mining and production technologies. Notably, many iron ores can be directly utilized as oxygen carriers following simple treatment [43]. Furthermore, due to the significant advantages of Fe-based oxygen carriers in terms of cost-effectiveness and environmental friendliness, they are widely applied in CLC technology. Leion et al. [44] confirmed the viability of natural ilmenite as an oxygen carrier in a small-scale fluidized bed using CO and H_2 as reactant gases. Furthermore, they utilized petroleum coke, wood chips, and two types of lignite as solid fuels to investigate the CLC efficiency of hematite when serving as an oxygen carrier. The results demonstrated that hematite maintained high reactivity. Moreover, its activity did not decrease as the reaction time increased [31]. Gu et al. [45,46] studied the feasibility of using hematite as an oxygen carrier for biomass and coal fuels in both a small-scale fluidized bed and a 1 kW_{th} continuous fluidized bed reactor. The experimental results demonstrated that hematite displayed high reactivity. Fraga-Cruz et al. [47] investigated the combustion mechanism of

ilmenite with syngas as the fuel and compared the air stream under varying temperature conditions. Berguerand et al. [16] conducted solid fuel CLC experiments using ilmenite in a 10 kW_{th} reactor, indicating that natural ilmenite can be employed as an oxygen carrier for continuous 22 h experiments in a 10 kW_{th} reactor. It displayed high reactivity, with the CO_2 capture efficiency ranging from 82.5% to 96%. Abad et al. [48] tested the performance of an Fe-based oxygen carrier at 800–950 °C for 40 h. The results showed that there was no decrease in particle reactivity, and agglomeration and carbon deposition were not observed. However, the relatively low mechanical stability of Fe-based oxygen carriers remains a bottleneck, limiting their large-scale application, and efforts to improve this reaction rate have been a key focus of research on CLC technology [49]. Wang et al. [50] studied the reaction characteristics of the synthesized CuO/Al_2O_3 and Fe_2O_3/Al_2O_3 oxygen carriers by combusting them with Chinese anthracite. It can be concluded that the CuO/Al_2O_3 is more suitable for the combustion process of anthracite. Shen et al. [51] demonstrated that potassium- and nickel-doped iron ore oxygen carriers enhance solid-fuel gasification in fluidized beds. Ni-doped Fe-based carriers also maintained high CO_2 capture efficiency in a 1 kW_{th} reactor [52]. Pérez-Méndez et al. [47] compared the performance of the ilmenite with other oxygen carriers used in CLC. It was concluded that ilmenite was the best available oxygen carrier for CLC processes due to its cost-effectiveness, environmental friendship, high methane conversion efficiency, and abundant natural availability. Ilmenite is among the most promising Fe-based oxygen carriers for commercial CLC deployment [30,53–55]. In addition, the attrition of the oxygen carrier represents another essential property that needs to be taken into account for its practical implementation in CLC systems [56]. The attrition resistance of the oxygen carrier directly affects its lifespan, which is a vital determinant in the scalability and economic viability of CLC technology. For Fe-based oxygen carriers in a fluidized bed reactor, as the reaction proceeds, the active components on the surface of the oxygen carrier are susceptible to attrition. This leads to a decrease in the content of these active components and subsequently modifies the reaction kinetics of the Fe-based oxygen carrier. Li et al. [57] explored the attrition characteristics of hematite under diverse conditions and observed that increasing the temperature can enhance the wear resistance of hematite under fluidized bed conditions. Hatanaka et al. [58] observed increasing ilmenite attrition rates over 150 redox cycles in a fluidized bed reactor. Unlike other Fe-based carriers, SEM revealed particle surface aggregation after 100–150 cycles, which was absent at 50 cycles. The observations of the samples using scanning electron microscopy and measurements of their tapped density and reduction rate showed that this rapid increase arises from changes in the surface morphology, including the migration of iron to the particle surfaces. Nelson et al. [59] explored the effects of temperature, fuel gas concentration, and flow rate on the properties of ilmenite and found that the fuel gas concentration affects the particle morphology evolution, and higher fuel gas concentration promotes the migration of iron to the surface of the ilmenite particles. Shen et al. [60] conducted long-term redox cycles of ilmenite using FB-TGA and found that during the reaction, iron migrates toward the particle surface, resulting in the formation of an iron-rich external shell.

Moreover, the reaction kinetics of the oxygen carrier are closely related to parameters such as the solid circulation rate between reactors and the solid inventory in each reactor. The solid circulation rate affects the contact time between the oxygen carrier and the fuel, which in turn influences the reaction rate. A proper solid circulation rate needs to be determined based on the reaction kinetics to achieve efficient combustion. Similarly, solid inventory governs the overall reaction rate and fuel conversion efficiency. Insufficient solid inventory results in inadequate oxygen carrier-fuel interaction, causing incomplete combustion. Conversely, excessive inventory can lead to challenges such as poor fluidization

and elevated pressure drops. Therefore, a comprehensive understanding of the reaction kinetics of the oxygen carrier is vital for the successful operation and development of CLC systems [61]. Furthermore, kinetic parameters are crucial for reactor design and reaction mechanism prediction. The redox reaction kinetic models of the oxygen carrier are key tools for exploring the underlying mechanisms of the carrier reaction and are essential for optimizing the oxygen carrier reaction process [22]. Investigating the redox kinetics of the oxygen carrier is critical for advancing CLC technology. Ei-Geassy [62] and Et-Tabirou [63] carried out experimental investigations to determine the activation energy for the reaction between Fe_2O_3 single crystals and CO. Wang et al. [64] analyzed the reduction behavior of Fe_2O_3/Al_2O_3 using thermogravimetric analysis (TGA). Breault et al. [65] conducted kinetic experiments regarding the reaction of hematite with CO in a TGA reactor to acquire the relevant kinetic parameters. Chen et al. [66] utilized a micro-fluidized bed reactor to investigate the reaction characteristics and kinetics of the reaction between hematite and CO. Zhang et al. [67] used an innovative pressurized fluidized bed reactor to obtain activation energies and pre-exponential factors for the reaction of Fe_2O_3 and Fe_2O_3/Al_2O_3 with CO. Garcia-Labiano et al. [68] studied the reaction kinetics of Cu-based, Fe-based, and Ni-based oxygen carriers with CO, H_2, and CH_4. Abad et al. [69] utilized the unreacted shrinking core model to depict the reaction of Fe_2O_3/Al_2O_3 with syngas. Su et al. [70] determined the intrinsic reaction kinetics of hematite by altering the temperature and gas concentrations in a TGA and a batch fluidized bed reactor.

Understanding the kinetics of oxygen carrier redox reactions is crucial for the modeling and the detailed design of CLC reactors. At present, a substantial amount of research has been conducted on the kinetics of Fe-based oxygen carrier reactions. However, different researchers have reached diverse conclusions, and there is a scarcity of articles that classify the kinetics of Fe-based oxygen carrier reactions based on distinct experimental conditions. Therefore, this review emphasizes the research progress regarding the reaction kinetics of Fe-based oxygen carriers, summarizing the effects of temperature, gas species, and gas concentration on their reaction kinetics. Additionally, the impacts of different reactors and various types of Fe-based oxygen carriers (both natural and synthetic) on the reaction kinetics are analyzed. Finally, the interactions between different fuel ashes and Fe-based oxygen carriers are also summarized. The present review may provide a theoretical foundation for the design of reactors based on Fe-based oxygen carriers.

2. Reaction Kinetics of Fe-Based Oxygen Carriers

In the study of CLC, the investigation of the reaction kinetics of the chemical reactions involved in the oxygen-carrying particles is helpful in revealing the main factors affecting the reaction performance of the oxygen carrier, enabling effective prediction of its reaction rate and providing the basic parameters required for numerical simulation using kinetic analysis, thereby guiding reactor design and simulation [68,71–74]. In practical CLC reactor systems, reactions involving oxygen carriers primarily involve gas–solid interactions. Gas–solid reactions can be categorized into catalytic and non-catalytic types. In catalytic gas–solid reactions, the primary chemical changes occur in the gas phase, while the solid phase acts as a catalyst. In non-catalytic gas–solid reactions, the solid reactants are gradually consumed as the reaction progresses, forming a solid product layer on their surface. These processes are collectively termed gas–solid reactions [75].

2.1. Kinetic Models of Fe-Based Oxygen Carrier Reaction

In order to predict the kinetic behavior of oxygen carrier reduction, different gas–solid reaction models have been proposed to explain the reaction mechanisms of oxygen carriers. At present, reaction models commonly used in CLC include the changing grain

size model, the shrinking core model, and the nucleation and nuclei growth model. The particle/grain evolution described for these three different reaction mechanism models in the reaction is shown in Figure 1, as described in Ref. [8]. Furthermore, numerous scholars have proposed modified reaction models for different reaction conditions to be applied in actual experiments. Examples include the apparent model [76], grain model [77], pore model, and rate equation theory [75].

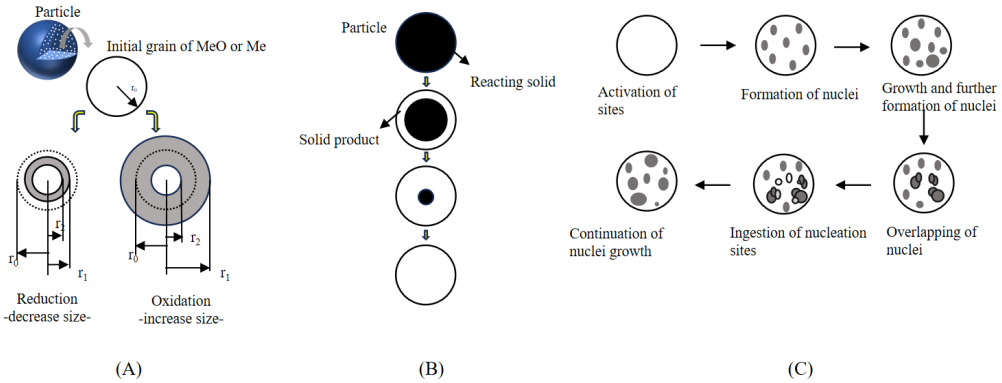


Figure 1. Evolution of particles/grains as described by different reaction mechanism models: (**A**) changing grain size model; (**B**) shrinking core model; (**C**) nucleation and nuclei growth model.

The selection of various kinetic models can significantly influence the kinetic parameters derived from reaction data. Habermann et al. [78] divided the reduction reaction of iron ore into two phases using a fluidized bed reactor: a first phase controlled by gas phase diffusion and a second phase dominated by the reduction reaction within the iron ore. Zhu [79] obtained the kinetic parameters of three models by choosing three different models at the same temperature. Mei et al. [80,81] researched the reaction between Fe_2O_3/Al_2O_3 and CO by dividing the reaction into two stages by converting the conversion rate, thus obtaining a mechanism model that was adapted to different stages. Ksepko et al. [82] determined the kinetic parameters of Fe_2O_3/TiO_2 using three different models to obtain different kinetic parameters. Monzam et al. [83] proposed a kinetic model based on two parallel reactions to describe the reduction of Fe_2O_3 to FeO; however, this model was constrained by CH_4 concentration and temperature conditions. Su et al. [70,84] examined the reduction kinetics of hematite with CO using TGA and a small-scale fluidized bed reactor. They found that the reduction of hematite occurs in two stages ($Fe_2O_3 \rightarrow Fe_3O_4$, $Fe_3O_4 \rightarrow FeO$), with the first stage being controlled by gas diffusion and the second stage by chemical reaction. Piotrowski et al. [85,86] researched the kinetics of the reduction reaction of hematite with syngas and obtained activation energies in the range of 25–125 kJ/mol using a two-dimensional nucleation and nuclei growth model. Consequently, for redox reactions, different models are required due to the different ways in which the structure of the solid particles changes. Notably, Li et al. [87,88] successfully predicted the kinetics of CaO carbonation under diverse experimental conditions by formulating a general rate equation theory. The approximate flowchart is shown in Figure 2. Moreover, based on the general rate equation theory, his team successfully predicted the H_2 and CO reduction kinetics of $CaMn_{0.775}Ti_{0.125}Mg_{0.1}O_{2.9-\delta}$ at different temperatures and concentrations by applying the transition state theory and density functional theory. They also predicted the reduction kinetic of Fe_2O_3 with H_2 at different temperatures and concentrations [89,90].

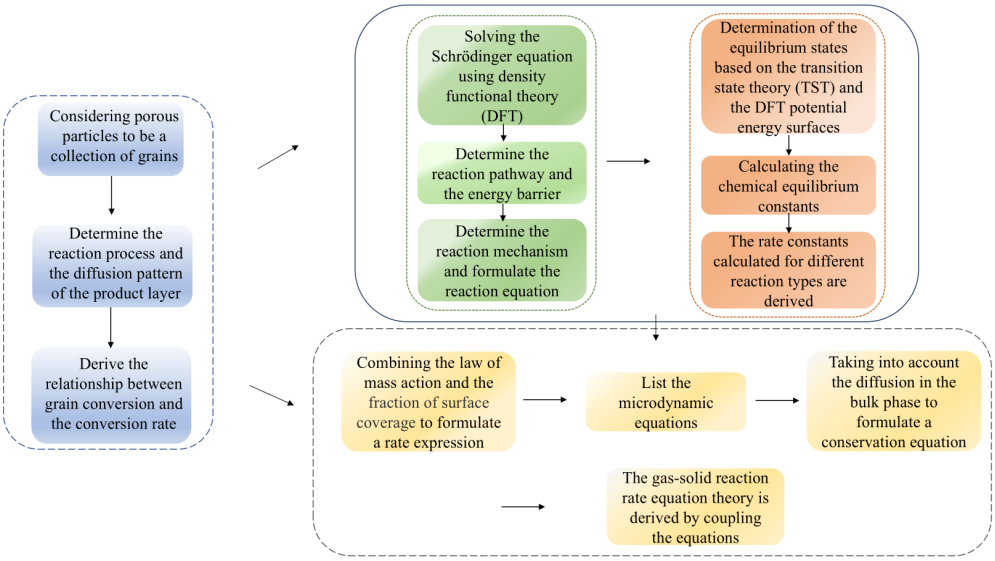


Figure 2. Flowchart of the derivation of the rate equation theory, as described in Ref. [75].

2.2. Reaction Kinetics of Fe-Based Oxygen Carriers in the TGA

Currently, the primary experimental devices for investigating the reaction kinetics of oxygen carriers include TGA [84,91], micro-fluidized bed reactor (MFB) [92,93], and fluidized bed thermogravimetric analysis (FB-TGA) [94,95]. The schematic diagrams of these experimental setups are illustrated in Figure 3. TGA, which is characterized by high measurement precision and excellent sensitivity, is the most representative and widely used analytical instrument for characterizing reaction kinetics [94]. The studies on the reaction kinetics of Fe-based oxygen carriers conducted using TGA are summarized in Table 3.

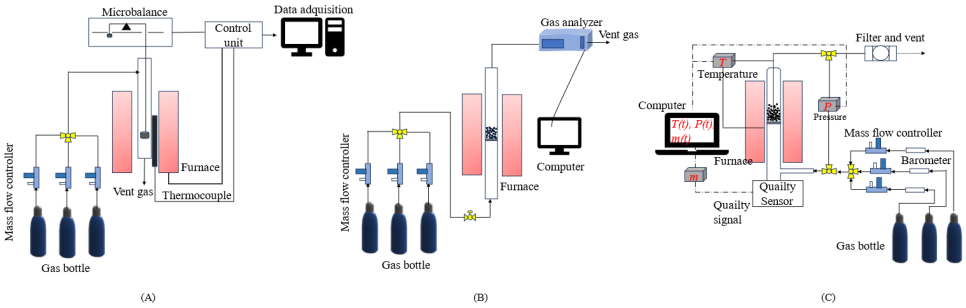


Figure 3. Schematic diagram of experimental equipment: (**A**) TGA; (**B**) MFB; (**C**) FB-TGA.

Table 3. A summary of reaction kinetics of Fe-based oxygen carrier using TGA as an experimental device.

Author	Oxygen Carrier	Reaction Gas	Ref.
Wang	Low-grade iron ore	CO, CH_4	[96]
Zhu	Pure Fe_2O_3, Fe_2O_3/Al_2O_3	CO	[97]
Zhao et al.	Pure Fe_2O_3, hematite, steel slag	O_2/CO_2	[98]
Mei et al.	Fe_2O_3/Al_2O_3	CO	[81]
Abad et al.	Ilmenite	H_2, CO, CH_4, O_2	[74]
Liu	Fe_2O_3/Al_2O_3	CO	[99]
Kespko et al.	Fe_2O_3-CuO/Al_2O_3, Fe_2O_3/TiO_2	Air, H_2	[82]
Bao et al.	Modified ilmenite	CO	[61]
Liu et al.	Ilmenite	CO	[100]
Piotrowski et al.	Hematite	CO, H_2	[85,86]

Table 3. *Cont.*

Author	Oxygen Carrier	Reaction Gas	Ref.
Su et al.	Hematite	CO	[70,84]
Ksepko et al.	Sinai ore	CH_4, O_2	[101]
Steiner et al.	Synthetic ilmenite	H_2	[102]
Khakpoor et al.	Ilmenite	CH_4	[103]
Dilmac	Iron ore	CO	[104]
Luo et al.	Pure Fe_2O_3, iron ore, $Fe_2O_3/MgAl_2O_4$	CH_4	[105]
Mendiara et al.	Tierga iron ore	H_2, CO, CH_4, O_2	[106]
Nasr et al.	Iron ore	CH_4	[107]
Cabello et al.	Fe_2O_3/Al_2O_3	CH_4, H_2, CO	[108]
Li et al.	Cu/Fe-based oxygen carrier	H_2	[109]
Monazam et al.	Hematite	CO	[65]
Abad et al.	Ilmenite	CH_4, H_2, CO, O_2	[74]
Moed et al.	Fe_2O_3-CuO/Al_2O_3	H_2, CO	[110]
Li et al.	Mn-Fe_2O_3	CO	[111]
Wang et al.	Fe_2O_3	CO/CO_2	[112]
Choisez et al.	Iron powder	H_2	[113]
Chai et al.	Iron powder	H_2	[114]
Halim et al.	Fe_2O_3 powder	H_2	[115]

2.3. Reaction Kinetics of Fe-Based Oxygen Carriers in Fluidized Bed Reactors

As discussed in Section 2.2, TGA is the most prevalently employed instrument for characterizing reaction kinetics. However, due to its measurement principle and structural characteristics, TGA suffers from issues such as low mass and heat transfer rates, non-uniform temperature distribution, and high gas diffusion resistance [116,117]. Meanwhile, there is a significant gradient in both the temperature and gas concentration within the particulate sample, which increases the deviation in characterization and kinetic fitting. It is far from the CLC process under bubbling and turbulent conditions [118]. Therefore, the reaction kinetics of oxygen carriers measured using TGA are often lower than the true values [22]. The employment of fluidized bed reactors to characterize gas–solid reaction kinetics not only facilitates the establishment of gas–solid contact patterns under diverse flow regimes but also enables the attainment of diffusion-enhanced isothermal reaction zones, which can closely mimic the actual process of CLC [94]. Thus, studies on the reaction kinetics of Fe-based oxygen carriers using fluidized bed reactors as the experimental equipment are summarized in Table 4.

Table 4. A summary of the reaction kinetics of an iron-based oxygen carrier using a fluidized bed reactor as an experimental device.

Author	Reactor	Oxygen Carrier	Reaction Gas	Ref.
Wu	Fluidized bed	Iron ore	CO	[119]
Schwebel et al.	Fluidized bed	Ilmenite	CO, CH_4, H_2	[120]
Su et al.	Fluidized bed	Hematite	CO	[70,84]
Perreault et al.	Micro-fixed bed	Ilmenite	CO	[121]
Yu et al.	Micro-fluidized bed	Hematite	CO/CO_2	[122]
Zhang et al.	Spouted bed	Fe_2O_3	CO/CO_2	[123]
Alsabak et al.	Fluidized bed	Laterite ore	H_2	[124]
Spreitzer et.al	Fluidized bed	Iron ore	H_2	[125]
Purnomo et al.	Fluidized bed	Ilmenite, iron sand, LD slag	CO, H_2, CH_4	[126]
Zhang et al.	Pressurized fluidized bed	Fe_2O_3, Fe_2O_3/Al_2O_3	CO	[67]

Table 4. *Cont.*

Author	Reactor	Oxygen Carrier	Reaction Gas	Ref.
Chiron et al.	Micro-fluidized bed	Fe-, Fe/Cu-based oxygen carriers	H_2	[127]
Cheng et al.	Fluidized bed	Fe_2O_3/Al_2O_3	H_2O, air	[128]
Feilmayr et al.	Fluidized bed	Hematite	H_2, CO, H_2O, CH_4, CO_2	[129]
Winayu et al.	Fluidized bed	$Fe_2O_3/Al_2O_3/SiO_2$	H_2, CO, CH_4	[130]
Habermann et al.	Fluidized bed	Iron ore	H_2, H_2O, CO, CO_2	[78]
Chen et al.	Micro-fluidized bed	Iron ore fines	CO	[66]
Winayu et al.	Fluidized bed	Ilmenite	CO, H_2, CH_4	[131]
Chen et al.	Micro-fluidized bed	Fe_2O_3	CO/CO_2	[132]
Zeng et al.	Homemade reactor	Fe_2O_3	H_2	[133]
Liu et al.	Honeycomb fixed bed	Fe_2O_3/Al_2O_3	H_2/CO	[134]

As shown in Tables 3 and 4, taking ilmenite as an example, Liu et al. [100] obtained an activation energy of 169.6 kJ/mol for the reaction of ilmenite with CO using TGA. Purnomo et al. [126] determined an activation energy in the range of 51–92 kJ/mol for the reaction between ilmenite and CO in a fluidized bed batch reactor, while Perreault et al. [121] reported an activation energy of 51 kJ/mol using a small-scale fluidized bed reactor. Similarly, Schwebel et al. [120] determined activation energies in the range of 71.59–89.34 kJ/mol within a batch fluidized bed reactor. Conversely, Winayu et al. [131] reported an activation energy of 25.54 kJ/mol. It is evident that the activation energies vary significantly across different reactor types, particularly when comparing results from conventional fluidized beds and small-scale fluidized beds. Moreover, it can be observed that for the same type of Fe-based oxygen carriers, different researchers have determined different kinetic parameters using TGA and fluidized bed reactors. Consequently, it is not recommended to directly apply the kinetic parameters derived from TGA to simulations associated with fluidized bed reactors.

However, in fluidized bed reactors, the reaction process must be estimated by measuring the concentrations of outlet gas components and performing inversion calculations. Even with high-resolution and fast-responsive mass spectrometers, it is difficult to achieve real-time and accurate TGA mass measurements. As a result, this method is unable to effectively distinguish between gas phase reactions and gas–solid reactions. Moreover, in fluidized bed reactors, phenomena like gas back-mixing and axial diffusion occur. These phenomena have the potential to distort the gas signal, thereby hindering the obtainment of the true kinetic information of the oxygen carrier [135]. Consequently, some researchers have sought to balance the strengths and weaknesses of TGA and fluidized bed reactors. By employing a fluidized bed thermogravimetric analysis, they integrate the efficient heat and mass transfer within the fluidized bed with the precise process measurement capabilities of TGA. This approach enabled novel research pathways and advanced analytical techniques for characterizing gas–solid reactions in CLC [94].

The École Polytechnique de Montréal in Canada first proposed the design and construction of a fluidized bed thermogravimetric analyzer in 2014. They developed two distinct FB-TGA systems: one heated using an electric furnace and another with magnetic induction [136–138]. Despite the limited measurement precision, it has determined the basic configuration and testing methods of the FB-TGA. The team led by Zhenshan Li from Tsinghua University [139,140] developed a micro-fluidized bed reactor in 2018. They verified the measurement feasibility of the FB-TGA and emphasized the advantages of the FB-TGA in characterizing rapid gas–solid reaction processes. The team led by Laihong Shen from Southeast University [141,142] developed an FB-TGA capable of introducing

steam using aerodynamic methods in 2020. Consequently, some scholars have initiated the study of the reaction kinetics of oxygen carriers using FB-TGA. Liu et al. [143] examined the oxygen uncoupling and redox reaction kinetics of perovskite-type oxygen carriers using a micro-fluidized bed thermogravimetric analyzer. They discovered that the oxidation reaction takes place only in the initial stage and is governed by the chemical reaction. The reduction reaction encompasses a fast phase and a slow phase, which are governed by the chemical reaction and the diffusion through the product layer, respectively. Wang et al. [144] explored the redox reaction kinetics of Fe/Cu-based oxygen carriers employing a micro-fluidized bed thermogravimetric analyzer. They characterized the redox reaction process in terms of the product island-based rate equation theory. Shen et al. [145] employed a fluidized bed thermogravimetric reactor to develop a multi-scale kinetic model for the analysis of the redox reaction kinetics of hematite.

3. Effect of Different Reaction Conditions on the Reaction Kinetics of Fe-Based Oxygen Carriers

3.1. Reaction Kinetics of Natural Fe-Based Oxygen Carriers

Natural ores represent a viable option due to their cost-effectiveness, availability, and satisfactory performance [146]. Ma et al. [147] utilized natural hematite as the oxygen carrier within a 50 kW_{th} coal-fired CLC reactor. They discovered that the maximum CO_2 capture efficiency attained 91%, with a combustion efficiency of 86% at 1000 °C. Berguerand et al. [16] conducted solid fuel CLC experiments using ilmenite in a 10 kW_{th} reactor. The study indicated that natural ilmenite could serve as an oxygen carrier in a 10 kW_{th} reactor. The ilmenite underwent a continuous operation for 22 h, exhibiting high reaction activity and CO_2 capture efficiencies ranging from 82.5% to 96%. Huang et al. [148] used natural hematite as the oxygen carrier in a fluidized bed reactor for direct chemical looping reforming of biomass. Their research found that hematite was able to supply oxygen. However, as the number of circulation cycles increased, particle wear and agglomeration were observed, leading to a decline in the oxygen carrier's reactivity. Ge et al. [149,150] employed hematite as the oxygen carrier in both a 25 kW intermittent reactor and a continuous reactor for chemical looping reforming of biomass to generate hydrogen. The research findings suggested that the presence of hematite accelerates the biomass gasification process, enhancing both the carbon conversion rate and the gasification rate. Consequently, numerous researchers have investigated the reaction kinetics of natural ores as oxygen carriers. Abad et al. [74] determined the reaction kinetics of pre-oxidized and activated ilmenite with H_2, CO, and CH_4 using TGA. Piotrowski et al. [86] and Feilmayr et al. [129] obtained the reaction kinetics of hematite with CO using TGA and a fluidized bed reactor, respectively. The research on the reaction kinetics of natural Fe-based oxygen carriers is summarized in Table 5.

Table 5. Summary of studies on the reaction kinetics of natural Fe-based oxygen carriers.

Author	Oxygen Carrier	Reaction Gas	Reactor	Kinetic Parameters		Ref.
				Activation Energy (kJ/mol)	Preexponential Factor	
Wang	Low-grade iron ore	CO, CH_4	TGA	CO: 56 CH_4: 62	CO: 1.5×10^{-3} CH_4: 2.7×10^{-4}	[96]
Schwebel et al.	Ilmenite	CO CH_4 H_2	Batch fluidized bed	CO: 71.59–89.35 CH_4: 146.90–186.75 H_2: 16.02–17.52	CO: 0.23–1.4 CH_4: 476.84–27,563.78 H_2: 0	[120]
Piotrowski et al.	Hematite	CO	TGA	58.13		[86]
Perreault et al.	Ilmenite	CO	Micro-fixed bed	51		[121]

Table 5. *Cont.*

Author	Oxygen Carrier	Reaction Gas	Reactor	Kinetic Parameters		Ref.
				Activation Energy (kJ/mol)	Preexponential Factor	
Yu et al.	Hematite	CO/CO_2	Micro-fluidized bed	49.64	6.55 s^{-1}	[122]
Ksepko et al.	Sinai ore	CH_4 O_2	TGA	CH_4: 35.3 O_2: 16.7	CH_4: 2.4×10^{-2} s^{-1} O_2: 1.02×10^{-4} s^{-1}	[101]
	Ilmenite	CH_4 O_2	TGA	CH_4: 62.4 O_2: 125.7	CH_4: 2.21×10^{-3} s^{-1} O_2: 129 s^{-1}	[70]
Khakpoor et al.	Ilmenite	CH_4 O_2	TGA	106.7 ± 10.6	9.43×10^{-1}	[103]
Dilmac	Iron ore	CO	TGA	40–65		[104]
Nasr et al.	Iron ore	CH_4	TGA	215	2.87×10^{8} min^{-1}	[107]
Liu et al.	Ilmenite	CO	TGA	169.6	1328.4 $L^{1.2}$ $mol^{-1.2}$ s^{-1}	[100]
Luo et al.	Iron ore	CH_4	TGA	183.63		[105]
Zhao et al.	Hematite	O_2/CO_2	TGA	78.43	1.04×10^{4}	[98]
Wu	Iron ore	CO	Fluidized bed	25.84–45.66	5.62×10^{-4}–4.96×10^{-3}	[119]
Alsabak et al.	Laterite ore	H_2	Fluidized bed	10.18–34.76		[124]
Spreitzer et al.	Iron ore	H_2	Fluidized bed	11–55		[125]
Purnomo et al.	Ilmenite	CO H_2 CH_4	Fluidized bed	CO: 91.6 H_2: 251 CH_4: 211	CO: 0.003 H_2: 1×10^{5} CH_4: 137	[126]
Feilmayr et al.	Hematite	H_2 CO H_2O CH_4 CO_2	Fluidized bed			[129]
Habermann et al.	Iron ore	H_2 CO CO_2 H_2O	Fluidized bed			[78]
Chen et al.	Fire iron ore	CO	Micro-fluidized bed	29.1–60.872	0.4053–18.681	[66]
Winayu et al.	Ilmenite	CO H_2	Fluidized bed	CO: 25.54 H_2: 63.11	CO: 3.72×10^{5} H_2: 779	[131]
Monazam	Hematite	CO	TGA	19.0 ± 0.14		[65]
Abad et al.	Activated ilmenite	CO H_2 CH_4 O_2	TGA	CO: 80.7 ± 2.4 H_2: 65.0 ± 2.7 CH_4: 135.2 ± 6.6 O_2: 25.5 ± 1.2	CO: 1.0×10^{-1} mol^{1-n} m^{3n-2} s^{-1} H_2: 6.2×10^{-2} mol^{1-n} m^{3n-2} s^{-1} CH_4: 9.8 mol^{1-n} m^{3n-2} s^{-1} O_2: 1.9×10^{-3} mol^{1-n} m^{3n-2} s^{-1}	[74]
	Pre-oxidized ilmenite	CO H_2 CH_4 O_2		CO: 113.3 ± 3.0 H_2: 109.32 ± 2.3 CH_4: 165.2 ± 12.4 O_2: E_{chr}: 11.8 ± 0.1 E_{dif}: 77.4 ± 0.3	CO: 2.1×10^{-1} mol^{1-n} m^{3n-2} s^{-1} H_2: 5.1×10^{-1} mol^{1-n} m^{3n-2} s^{-1} CH_4: 8.8 mol^{1-n} m^{3n-2} s^{-1} O_2: k_{s0}: 8.0×10^{-5} mol^{1-n} m^{3n-2} s^{-1} D_{e0}: 1.37×10^{-5} mol^{1-n} m^{3n-2} s^{-1}	
Liu	Wüstite	H_2 CO	Fluidized bed	H_2: 62–79 CO: 66–83	H_2: 0.63–1.8 s^{-1} CO: 0.099–2.7 s^{-1}	[151]
Khani et al.	Hematite	H_2	TGA	40.87		[152]

3.2. Reaction Kinetics of Synthetic Fe-Based Oxygen Carriers

However, natural ores are unable to satisfy the mechanical stability requirements of pilot-scale CLC units. To acquire oxygen carriers with mechanical properties and stability, various oxygen carriers have been synthesized artificially, including Fe-based, Ni-based, Cu-based, Mn-based, and composite oxygen carriers [22]. Yang et al. [153] confirmed using TGA that a 20% mass ratio of copper ore to iron ore could produce a synergistic effect on

the reaction between the oxygen carrier and coal. Ryden et al. [154] incorporated 0.6 wt% NiO into ilmenite and performed the reaction in a 100 kW_{th} coal-fired CLC reactor. As a result, the combustion efficiency increased from 76% to 90%. Tobias et al. [155] added Ni to various types of Fe_2O_3 particles and subjected them to multiple redox cycles in CLC. They found that the type of inert carrier and the calcination temperature significantly influenced the reactivity of the oxygen carrier. Yang et al. [156] investigated the CLC cycle of coal using hematite modified with copper as the active component. They reported that the addition of 6% copper significantly enhanced the reactivity of hematite. Jiang et al. [157] synthesized an oxygen carrier using an admixture of hematite and CuO. It has been discovered that the reactivity of the new oxygen carrier increases with the number of cycles. Bao et al. [92,158] observed carbon deposition and slag formation in CLC experiments using pure Fe_2O_3 oxygen carriers, whereas no agglomeration occurred with the addition of 10 mol% Al_2O_3. In addition, a new ilmenite oxygen carrier was synthesized by impregnating the original ilmenite particles with K_2CO_3, Na_2CO_3, or $Ca(NO_3)_2$, and its cyclic reduction reactivity was investigated in a fluidized bed reactor. It was found that the addition of foreign ions significantly enhanced the reduction reactivity of ilmenite. Synthetic oxygen carriers often demonstrate superior performance compared to natural oxygen carriers, likely due to the synergistic effects among composite oxygen carriers [159], which enhance their reaction rates. Consequently, the reaction kinetics parameters of synthetic oxygen carriers differ from those of natural Fe-based oxygen carriers. As shown in Table 6, the reaction kinetics of Fe-based oxygen carriers synthesized using methods such as adding supporting materials are summarized. The materials currently employed for investigating the reaction kinetics of Fe-based oxygen carriers are illustrated in Figure 4.

Table 6. Summary of studies on the reaction kinetics of synthetic Fe-based oxygen carriers.

Author	Oxygen Carrier	Reaction Gas	Reactor	Kinetic Parameters		Ref.
				Activation Energy (kJ/mol)	Preexponential Factor	
Zhu	Fe_2O_3/Al_2O_3	CO	TGA	74.42	0.525×10^5	[97]
Mei et.al	Fe_2O_3/Al_2O_3	CO	TGA	131–270	3.1×10^3–1.6×10^{12}	[81]
Liu	Fe_2O_3/Al_2O_3	CO	TGA			[99]
Kespko et al.	Fe_2O_3-CuO/Al_2O_3 Fe_2O_3/TiO_2	Air, H_2	TGA	41.318–42.594 33.08–35.379	0.027–0.255 0.056–0.069	[82]
Bao et al.	Modified ilmenite	CO	TGA			[61]
Steiner et al.	Synthetic ilmenite	H_2	TGA	15–80		[102]
Luo et al.	$Fe_2O_3/MgAl_2O_4$	CH_4	TGA	79.96		[105]
Cabello et al.	Fe_2O_3/Al_2O_3	CH_4 H_2 CO O2	TGA	CH_4: 66 H_2: 8 CO: 14 O_2: 23	CH_4: 4.34×10^1 H_2: 1.45×10^{-1} CO: 1.59×10^{-1} O_2: 3.64×10^{-1}	[108]
Li et al.	Cu/Fe-based oxygen carrier	H_2	TGA	59.07	6.69×10^2	[109]
Moed et al.	Fe_2O_3-CuO/Al_2O_3	H_2 CO	TGA	H_2: 32.2–54.1 CO: 6.6–17.1		[110]
Li et al.	Mn-Fe_2O_3	CO	TGA	315.4–907.8	9.65×10^{18}–4.49×10^{48}	[111]
Zhang et al.	Fe_2O_3/Al_2O_3	CO	Pressurized fluidized bed	101 ± 14	1.8×10^{-3}	[67]

Table 6. *Cont.*

Author	Oxygen Carrier	Reaction Gas	Reactor	Kinetic Parameters		Ref.
				Activation Energy (kJ/mol)	Preexponential Factor	
Chiron et al.	Cu-Fe oxygen carrier	H_2	Micro-fluidized bed	46 51		[127]
Cheng et al.	Fe_2O_3/Al_2O_3	H_2O, Air	Fluidized bed reactor		0.0026–0.0118	[128]
Winayu et al.	$Fe_2O_3/Al_2O_3/SiO_2$	H_2 CO CH_4	Fluidized bed	H_2: 41.4 CO: 79.2 CH_4: 13.6	H_2: 27.7 CO: 712 CH_4: 0.947	[130]
Alberto et al.	Fe_2O_3/Al_2O_3	CO	TGA	20	2.5×10^{-4} mol^{1-n} m^{3n-2} s^{-1}	[69]
Jin et al.	Ni-Fe-Zr oxygen carrier	H_2 CO_2	TGA	H_2: $Fe_2O_3 \rightarrow$ FeO:14.90–20.00 FeO → Fe:13.87–25.40 CO_2: 46.22–55.28	H_2: $Fe_2O_3 \rightarrow$ FeO: 3.05–6.06 FeO → Fe: 0.45–1.55 CO_2: 55.19–186.85	[160]
Zhang et al.	Fe_2O_3/Al_2O_3	CO	Pressurized fluidized bed	Cycle 2: 110 ± 12 Cycle 3: 115 ± 11 Cycle 4: 97 ± 13 Cycle 5: 101 ± 14	Cycle 2: 104.6 (−11.7 + 113.2) m s^{-1} Cycle 3: 211.4 (−21.6 + 24.1) m s^{-1} Cycle 4: 17.8 (−2.2 + 2.5) m s^{-1} Cycle 5: 33.2 (−4.5 + 5.2) m s^{-1}	[67]
Li et al.	xwt%Ni-Fe_2O_3/Al_2O_3 (x = 0, 5, 10, 20, 50)	CH_4	TGA	x = 0: 75.40 x = 5: 71.25 x = 10: 65.70 x = 20: 53.93 x = 50: 62.03	x = 0: 0.59 m^{3n} mol^{-n} s^{-1} x = 5: 0.75 m^{3n} mol^{-n} s^{-1} x = 10: 0.26 m^{3n} mol^{-n} s^{-1} x = 20: 0.11 m^{3n} mol^{-n} s^{-1} x = 50: 0.40 m^{3n} mol^{-n} s^{-1}	[161]
Liu et al.	Fe_2O_3/Al_2O_3	H_2/CO	Honeycomb fixed bed reactor	First stage: 3.5 Second stage:33.2	First stage: 3.06×10^{-5} Second stage: 2.99×10^{-4}	[134]

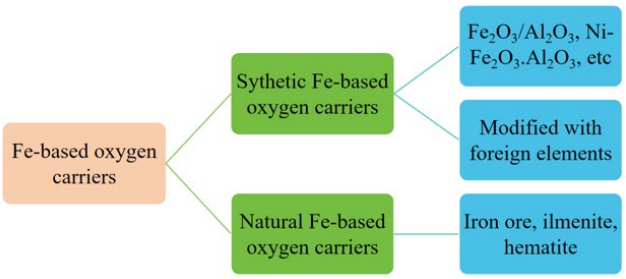


Figure 4. Materials commonly used in kinetic studies of Fe-based oxygen carriers.

Based on the data presented in Tables 5 and 6, Abad et al. [74] obtained an activation energy of 65.0 ± 2.7 kJ/mol for the reaction between ilmenite and H_2 using TGA. In contrast, Steiner et al. [102] reported an activation energy range of 15–80 kJ/mol for the reaction between synthetic ilmenite and H_2. Zhu [97] conducted TGA experiments to determine the activation energy of pure Fe_2O_3 and Fe_2O_3/Al_2O_3. This study found that the addition of an inert support did not change the reaction model but increased the activation energy of the reaction. This indicates that the presence of the inert support may affect the reaction kinetics, possibly due to changes in the surface area, pore structure, or mass transfer characteristics of the oxygen carrier. Similarly, Luo et al. [105] investigated the reaction between $Fe_2O_3/MgAl_2O_4$ and methane using TGA and reported that the activation energy for this reaction was higher than that for pure Fe_2O_3. Thus, it is evident that while the incorporation of inert supports can mitigate issues such as the sintering of Fe-based oxygen carriers at high temperatures and improve their cycle stability, it may also reduce the activity of the active components in the reactants. This reduction decreases the amount of active species required for the reaction, consequently increasing the activation energy.

3.3. Effect of Temperature and Gas Concentration on Reaction Kinetics of Fe-Based Oxygen Carriers

In CLC, temperature significantly influences reaction rates and chemical equilibrium. Gas concentration affects the frequency of effective collisions between reactants, thereby influencing the reaction rate. Therefore, the effects of varying temperatures and reaction gas concentrations on reaction kinetic parameters are of great significance. The literature reviews indicate that CO is among the most extensively studied reduction gases in current research. Taking ilmenite as an example, Abad et al. [74] obtained an activation energy of 113.3 ± 3.0 kJ/mol for CO concentrations ranging from 5 to 50% and temperatures in the range of 800–950 °C. Liu et al. [100] and Perreault et al. [121] obtained activation energies of 169.6 kJ/mol and 51 kJ/mol, respectively, for CO concentrations of 10–30% and 15–30%, respectively, and temperature ranges of 850–1050 °C and 800–900 °C, respectively. Similarly, Purnomo et al. [126] gained an activation energy of 59.4 kJ/mol for a CO concentration of 50% and temperatures ranging from 850 to 975 °C. Winayu et al. [131] gained an activation energy of 25.54 kJ/mol for a CO concentration of 25% and temperatures of 900–1000 °C. This demonstrates that the influence of gas concentration and temperature variations on the kinetic parameters of Fe-based oxygen carriers is significant and cannot be overlooked. With increasing temperature, the kinetic energy of reactant molecules increases correspondingly. This enhances collision intensity and frequency, leading to higher reaction rates. At low gas concentrations, the likelihood of collisions between reactants and gas molecules is reduced, resulting in slower reaction rates. As the concentration increases, collision frequency between reactants and gas molecules rises, thereby accelerating the reaction rate. Therefore, the effects of temperature and gas concentration variations on the reaction kinetics of Fe-based oxygen carriers are summarized in Table 7, using CO as the reduction gas.

Table 7. Research on the reaction kinetics of Fe-based oxygen carriers by varying temperatures and gas concentrations with CO as the reducing gas.

Author	Oxygen Carrier	Gas Concentration	Temperature (°C)	Kinetic Parameters		Ref.
				Activation Energy (kJ/mol)	Preexponential Factor	
Wang	Low-grade iron ore	10%, 20%	850, 900, 950	56	1.5×10^{-3} mol^{1-n} m^{3n-2} s^{-1}	[96]
Zhu	Fe_2O_3	20%	750, 850, 950	52.46	0.7×10^{6} min^{-1}	[97]
Abad et al.	Ilmenite	5–50%	800, 850, 900, 950	113.3 ± 3.0	2.1×10^{-1} mol^{1-n} m^{3n-2} s^{-1}	[74]
Liu et al.	Ilmenite	10%, 20%, 30%	850, 950, 1050	169.6	1328.4 $L^{1.2}$ $mol^{-1.2}$ s^{-1}	[100]
Perreault et al.	Ilmenite	15%, 20%, 25%	800, 850, 900	51		[121]
Wu	Iron ore	5%, 7.5%, 10%, 12.5%	750–800 800–850 850–900	45.66 34.58 25.84	0.00496 s^{-1} 0.00143 s^{-1} 0.000562 s^{-1}	[119]
Su et al.	Hematite	15–50% 5–20% 5%, 7.5%, 15%	400–650 850, 900, 950, 1000 400–650	74.48 110.75 138.55	1.2×10^{12} s^{-1} 88.55 $m^{4.5}$ $mol^{-1.5}$ s^{-1} 6.8×10^{13} s^{-1}	[70,84,162]
Mei et al.	Fe_2O_3/Al_2O_3	50%	1000	131–270	3.1×10^{3}–1.6×10^{12} s^{-1}	[81]
Bao et al.	Modified ilmenite	11%	900			[61]
Dilmac	Iron ore	10%, 20%, 25%, 50%	750, 800, 850, 900	40–65		[104]
Wang et al.	Fe_2O_3	0–38%, 42–65%, 68–88%	800–900	35–70		[112]

Table 7. *Cont.*

Author	Oxygen Carrier	Gas Concentration	Temperature (°C)	Kinetic Parameters		Ref.
				Activation Energy (kJ/mol)	Preexponential Factor	
Mendiara et al.	Tierga iron ore	5–60%	800–1000	76.1 ± 6 139 ± 5	1.45×10^{-1} mol^{1-n} m^{3n-2} s^{-1} $9.16 \cdot 10^{-5}$	[106]
Cabello et al.	Fe_2O_3/Al_2O_3	5–60%	700–1050	14 204	1.59×10^{-1} 2.29×10^{9}	[108]
Monazam et al.	Hematite	5%, 10%, 20%	700–950	19.0 ± 0.14		[65]
Moed et al.	Fe_2O_3-CuO/Al_2O_3	20%	850, 875, 900, 925	6.6–13.8		[110]
Li et al.	Mn-Fe_2O_3		750, 800, 850	315.4–907.8	9.65×10^{18}–4.49×10^{48}	[111]
Purnomo et al.	Ilmenite iron sand LD slag	50%	850, 875, 900, 925, 950, 975	59.4 51.7 64.8	7.34 s^{-1} 0.73 s^{-1} 9.78 s^{-1}	[126]
Winayu et al.	Ilmenite $Fe_2O_3/Al_2O_3/SiO_2$	25%	900, 950, 1000	25.54 79.2	3.72×10^{5} 712 min^{-1}	[130, 131]
Bohn et al.	Fe_2O_3	8.5–9.5%	650–900	75.0–94.0		[163]
Chen et al.	Fe_2O_3	40%, 60%, 80%, 100%	750–950	$Fe_2O \rightarrow Fe_3O_4$: 30.60 ± 0.75 to 52.99 ± 0.78 $Fe_3O_4 \rightarrow FeO$: 52.44 ± 0.10 to 80.83 ± 0.12 $FeO \rightarrow Fe$: 45.74 ± 0.25–92.12 ± 0.27	$Fe_2O_3 \rightarrow Fe_3O_4$: 1.84 ± 0.69 s^{-1}–13.71 ± 5 34 s^{-1} $Fe_3O_4 \rightarrow FeO$: 17.57 ± 0.87 s^{-1}–426.47 ± 25.92 s^{-1} $FeO \rightarrow Fe$: 3.28 ± 0.41 s^{-1}–628.46 ± 84.40 s^{-1}	[132]
Chen et al.	Iron ore fines	50%	700–850	29.1–60.872	0.4053–18.681 s^{-1}	[66]

The reaction of oxygen carriers in CLC is a complex gas–solid non-catalytic reaction [22]. Therefore, the reactivity of oxygen carriers should be studied by taking into account the combined effects of their intrinsic chemical reaction factors and mass transfer factors. Intrinsic reaction kinetics refers to the reaction kinetics unaffected by fluid flow, mass transfer, and heat transfer. It describes the inherent laws governing the chemical reaction itself. Zhang et al. [67] conducted research using a pressurized fluidized bed reactor to investigate the reaction kinetics of Fe_2O_3 and Fe_2O_3/Al_2O_3 with CO. They established an intrinsic reaction kinetics model for this process. Piotrowski et al. [85,86] studied the reduction of hematite (Fe_2O_3) to magnetite (Fe_3O_4) and determined that the activation energy for this process ranges from 25 to 125 kJ/mol, with a reaction order of 1. They also concluded that a two-dimensional nucleation and growth model is more suitable for describing the overall reaction process. Pineau et al. [164] examined the reduction process of hematite with hydrogen at temperatures ranging from 220 to 730 °C. They reported that the activation energy for the first stage of the reaction, where Fe_2O_3 is reduced to Fe_3O_4, is 76 kJ/mol. For the second stage, where Fe_3O_4 is reduced to FeO, the activation energy was found to be 39 kJ/mol. Monazam et al. [65] used TGA to determine the reaction kinetic parameters for the reduction of hematite by CO. They found that the reduction process proceeds in two concurrent steps, with an activation energy of 19.0 ± 0.14 kJ/mol. Su et al. [70] investigated the intrinsic reaction kinetics of hematite reduction by CO. They determined that for temperatures ranging from 400 to 650 °C, the intrinsic activation energy for the first stage of the reaction, where Fe_2O_3 is reduced to Fe_3O_4, is 138.55 kJ/mol. This value implies a higher energy barrier for the initial reduction step compared to the findings of Monazam et al. [65], implying that the reaction kinetics may vary significantly depending on the specific experimental conditions and the nature of the reaction mechanism.

3.4. Research on the Interaction and the Effect of Properties of Ash with Fe-Based Oxygen Carrier

One of the most critical characteristics of an oxygen carrier is its ability to undergo oxidation and reduction, facilitating oxygen transfer within a chemical looping system. Highly reduced oxygen carriers may encounter various performance issues, such as reduced reactivity, agglomeration, and defluidization. Meanwhile, taking coal in solid fuels as an example, the accumulated coal ash deposited on the surface of the oxygen carrier not only blocks the pores and hinders gas–solid reactions but also causes sintering and agglomeration of the oxygen carrier [22]. Therefore, the interaction between ash and the oxygen carrier is an important issue in the CLC process. Thermodynamic calculations indicate that reactions between ash and the oxygen carrier can occur at high temperatures, but at a relatively low rate [165]. Additionally, in the CLC process, studies have shown that for Fe-based oxygen carriers, ash deposition on the oxygen carriers and the interactions between the ash and the carriers are inevitable, and the ash will react with the oxygen carriers [166–169], which exacerbates performance issues [170]. These interactions can lead to modifications in the physical and chemical properties of the oxygen carrier, potentially compromising its cyclic stability and efficiency. The reactions can alter the surface area, porosity, and mechanical strength of the oxygen carrier, which are all critical factors for the overall performance of the CLC system. However, the current CLC technology is unable to completely separate the oxygen carrier from the ash [171]. Zhou et al. [172] studied the influence of biomass ash on the performance of iron ore and found that the inorganic components present in biomass ash vary, leading to different effects on the reactivity of the iron ore. Ilyushechkin et al. [173] examined the interaction between two types of coal ash and Fe-based oxygen carriers. The results demonstrated that iron-rich ash enhances the oxidation and reduction kinetics of iron ore. While it does not affect the reduction kinetics of ilmenite, it significantly prolongs the oxidation time of ilmenite. Silica-rich ash reduces the oxidation rates of iron ore. Yan et al. [174] modified iron ore with rape stalk ash and wheat stalk ash and found that the cumulative CO conversion of biomass ash modified oxygen carriers was significantly higher than that of unmodified oxygen carriers. Gu et al. [175] confirmed the effect of adding biomass ash to the oxygen carrier on its performance and conducted experiments with the addition of 5%, 10%, 15%, and 20% ash. The results showed that the addition of only 5% of rape straw ash was effective in improving the reactivity of the iron ore oxygen carrier. Moreover, no decrease in reactivity was observed after adding 20% of the ash. Feng et al. [176] investigated the enhancement mechanism of alkali metal doping on the reactivity of Fe_2O_3 oxygen carriers using density functional theory (DFT) calculations. The results demonstrated that the smaller the ionic radius of alkali dopants and the stronger their electronegativity are, the higher the activity of surface oxygen at sites distal to the dopants. The surface oxygen adjacent to the dopants will show the better activity compared to the one away from the dopants. Gu et al. [45,177] first developed a K_2CO_3-modified Fe_2O_3 OC and reported that this modification significantly enhanced the carbon gasification rate and promoted the conversion of carbonaceous gases to CO_2 in the CLC process. Subsequently, they evaluated the reactivity of a 6% K_2CO_3-modified Fe_2O_3 with CO and H_2 in a TGA and demonstrated that K as an electric donor could weaken the Fe-O bond, enhancing its reactivity. Yang et al. [178] investigated the interaction between wheat straw ash (WSA) and ilmenite using a fixed bed reactor. The result revealed that ilmenite with 10 wt% wheat straw ash showed the best performance. It was inferred that $KFeO_2$ phase formation as a result of the interaction between WSA and ilmenite promotes the reactivity of the oxygen carrier. Therefore, the ash-doping experiments on Fe-based oxygen carriers are summarized in Table 8 to illustrate the effects of different types of ash on the performance of these oxygen carriers.

Table 8. Research on the interaction of iron-based oxygen carriers with ash.

Author	Oxygen Carrier	Ash	Conclusion	Ref.
Zhang et al.	Fe_2O_3/Al_2O_3	Three types of coal ash	When the oxygen carrier was in contact with coal ash having a high Ca content, its reactivity was significantly enhanced after several cycles. Coal ash with a high Si content had a detrimental effect on the oxygen carrier.	[179]
Bao et al.	Fe_2O_3/Al_2O_3	Four types of coal ash	Ash composed of $CaSO_4$ enhanced the activity of oxygen carrier, and the effect of ash in decreasing carrier activity increased with the number of cycles.	[167]
Zhou et al.	iron ore	Biomass ash	The K-rich ash generated K_3FeO_2, which improved the reducing activity of the iron ore.	[172]
Guo et al.	Fe_2O_3/Al_2O_3	Coal ash	The presence of ash exerted an inhibitory influence on the reduction reaction process from Fe_2O_3 to Fe_3O_4.	[180]
Ilyushechkin et al.	iron ore, ilmenite	Two types of coal ash (with Si, Fe, Mg)	The ash rich in Fe augmented the redox kinetics of iron ore while having no impact on ilmenite. The ash abundant in Si decreased the oxidation rate of iron ore.	[173]
Wang et al.	Fe_2O_3/Al_2O_3	Sludge ash	When the number of cycles was fewer than 10, the activity of the oxygen carrier had the potential to increase. As the number of cycles increased, the ash decreased the reactivity of the oxygen carrier.	[181]
Purnomo et al.	Nature ores, waste materials	Three K salts	The initial oxidation state of the surface of the oxygen carrier had only a limited influence on its interaction with K salts.	[170]
Cheng et al.	Pure Fe_2O_3	Coal ash, biomass ash	A small amount of ash promoted the reduction of Fe_2O_3. Moreover, Ca^{2+}, K^+, and Na^+ in ash interacted with silica-aluminate to form low melting point compounds.	[171]
Gu et al.	Iron ore	Three types of biomass ash	Ash that was rich in K and had a low Si content served to enhance fuel conversion.	[175]
Yang et al.	Ilmenite	Biomass ash	The reactivity of ilmenite first increased and then decreased as the amount of biomass ash added increased, reaching its peak at 10% biomass ash addition. The addition of 15% biomass ash led to severe particle sintering.	[178]
Yilmaz et al.	Pure Fe_2O_3	Synthetic biomass-derived ash (with K, Na)	The co-presence of K and Si in the ash increased agglomeration.	[182]
		Synthetic biomass-derived ash (with Mg, Ca)	Under the same experimental conditions, it was observed that Mg led to more severe clumping phenomena than Ca.	[183]

4. Conclusions and Future Prospects

This paper comprehensively reviews the effects of various factors on the reaction kinetic parameters of Fe-based oxygen carriers in CLC. It categorizes the findings according

to reactor type (including TGA, FB reactors, and FB-TGA), temperature, and atmosphere. The following conclusions and prospects can be drawn.

(1) The measurement methods for characterizing the reaction kinetics of oxygen carriers primarily include TGA, FB reactors, and FB-TGA. For the Fe-based oxygen carriers, TGA determines kinetic parameters by tracking mass changes in real-time; however, it faces challenges such as low mass and heat transfer rates. In contrast, FB reactors evaluate the reaction process and derive kinetic parameters by measuring the concentration of gas components at the outlet. However, it is difficult to achieve real-time and accurate measurements compared with TGA. The activation energy derived from TGA could differ significantly from that obtained using fluidized bed reactors; hence, kinetic parameters obtained from TGA are not advisable for direct application in fluidized bed simulations.

(2) A distinction exists between intrinsic and apparent reaction kinetics. Existing studies on intrinsic reaction kinetics primarily focus on pure Fe_2O_3, hematite, and ilmenite, and a broad investigation on the widely utilized materials is required.

(3) Due to the relatively low mechanical stability of Fe-based oxygen carriers, a common strategy to enhance the reaction performance of Fe-based oxygen carriers is the incorporation of inert supports. The addition of inert supports can alleviate problems such as the sintering of Fe-based oxygen carriers at high temperatures and improve their cyclic stability. However, partially inert supports may impose a restrictive effect on the active component Fe_2O_3 in the Fe-based oxygen carrier, thereby influencing the amount of active components required for the reaction. Consequently, the apparent activation energy is generally higher than that of pure Fe_2O_3.

(4) In FB reactors, attrition is a critical factor affecting the service life of Fe-based oxygen carriers. Specifically for ilmenite, during the reaction process, active iron components migrate to the surface, while particle collisions within the FB reactor may lead to attrition, resulting in a decrease in active component content and the reaction kinetics. However, research on the impact of attrition on the reaction kinetics of Fe-based oxygen carriers remains limited, necessitating the need for further investigation.

(5) During the long-term operation of CLC, it is inevitable that solid fuel ash interacts with the oxygen carrier, leading to physical and chemical changes in the carrier. The interactions may affect the reaction kinetics of the oxygen carrier. Existing studies primarily focus on the mechanisms of ash–oxygen carrier interactions and their effects on the surface morphology of oxygen carriers, while investigations into their impact on reaction kinetics are required. Current studies on the interaction between ash and Fe-based oxygen carriers have primarily focused on two aspects: microstructural modifications after adding ash, which are analyzed using DFT calculations, and alterations in reaction mechanisms and reactivities after adding ash, which are evaluated using experimental studies. However, few studies have integrated the results based on DFT calculations with experimental results to explore the interactions of ash and oxygen carriers. It is recommended to combine experimental and DFT methodologies to systematically elucidate the influences of ash on the kinetics of Fe-based oxygen carriers in future work.

Author Contributions: Conceptualization, D.L.; investigation, S.Q., Z.L., T.-y.M. and R.-G.K.; writing—original draft preparation, S.Q., T.Z., J.M. and X.Y.; writing—review and editing, D.L., Z.L., H.Y., M.Z. (Man Zhang), T.-y.M., R.-G.K., X.Z. and H.W.; supervision, D.L. and H.W.; project administration, D.L. and M.Z. (Mingyu Zhang); funding acquisition, D.L. and X.Z. All authors have read and agreed to the published version of the manuscript.

Funding: This work is supported by the National Natural Science Foundation (Grant No. 52266007), Yunnan Fundamental Research Projects (Grant No. 202201BE070001-011), and Yunnan Major Scientific and Technological Projects (Grant No. 202405AO120103).

Data Availability Statement: The original contributions presented in this study are included in the article. Further inquiries can be directed to the corresponding authors.

Conflicts of Interest: Authors Xi Yang and Mingyu Zhang were employed by the company Yunnan Energy Research Institute Co., Ltd. The remaining authors declare that the research was conducted in the absence of any commercial or financial relationships that could be construed as a potential conflict of interest.

References

1. Dai, A.; Fyfe, J.C.; Xie, S.-P.; Dai, X. Decadal modulation of global surface temperature by internal climate variability. *Nat. Clim. Change* **2015**, *5*, 555–559.
2. Netz, B.; Davidson, O.R.; Bosch, P.R.; Dave, R.; Meyer, L.A. *Climate Change 2007: Mitigation. Contribution of Working Group III to the Fourth Assessment Report of the Intergovernmental Panel on Climate Change*; Intergovernmental Panel on Climate Change (IPCC): Geneva, Switzerland, 2007.
3. Zhao, H.; Tian, X.; Ma, J.; Chen, X.; Su, M.; Zheng, C.; Wang, Y. Chemical looping combustion of coal in China: Comprehensive progress, remaining challenges, and potential opportunities. *Energy Fuels* **2020**, *34*, 6696–6734.
4. Lyngfelt, A.; Brink, A.; Langørgen, Ø.; Mattisson, T.; Rydén, M.; Linderholm, C. 11,000 h of chemical-looping combustion operation—Where are we and where do we want to go? *Int. J. Greenh. Gas Control* **2019**, *88*, 38–56.
5. Adánez, J.; Abad, A. Chemical-looping combustion: Status and research needs. *Proc. Combust. Inst.* **2019**, *37*, 4303–4317.
6. Richter, H.J.; Knoche, K.F. Reversibility of combustion processes. In *Efficiency and Costing*; ACS Publications: Washington, DC, USA, 1983.
7. Ishida, M.; Zheng, D.; Akehata, T. Evaluation of a chemical-looping-combustion power-generation system by graphic exergy analysis. *Energy* **1987**, *12*, 147–154.
8. Adanez, J.; Abad, A.; Garcia-Labiano, F.; Gayan, P.; de Diego, L.F. Progress in chemical-looping combustion and reforming technologies. *Prog. Energy Combust. Sci.* **2012**, *38*, 215–282.
9. Arjmand, M.; Leion, H.; Mattisson, T.; Lyngfelt, A. Investigation of different manganese ores as oxygen carriers in chemical-looping combustion (CLC) for solid fuels. *Appl. Energy* **2014**, *113*, 1883–1894.
10. Ishida, M.; Jin, H. A new advanced power generation system using chemical-looping combustion. *Energy* **1994**, *19*, 415–422.
11. Lewis, W.; Gilliland, E.; Paxton, R. Low-temperature oxidation of carbon. *Ind. Eng. Chem.* **1954**, *46*, 1327–1331.
12. Ishida, M.; Jin, H. A novel combustor based on chemicallooping reactions and its reaction kinetics. *J. Chem. Eng. Jpn.* **1994**, *27*, 296–301.
13. Lyngfelt, A.; Leckner, B.; Mattisson, T. A fluidized-bed combustion process with inherent CO_2 separation;application of chemical-looping combustion. *Chem. Eng. Sci.* **2001**, *56*, 3101–3113.
14. Lyngfelt, A.; Kronberger, B.; Adanez, J.; Morin, J.X.; Hurst, P. The grace project: Development of oxygen carrier particles for chemical-looping combustion. Design and operation of a 10 kW chemical-looping combustor. In *Greenhouse Gas Control Technologies 7*; Elsevier: Amsterdam, The Netherlands, 2005; pp. 115–123.
15. Ryu, H.-J.; Jin, G.-T.; Yi, C.-K. Demonstration of inherent CO_2 separation and no NOx emission in a 50kW chemical looping combustor: Continuous reduction and oxidation experiment. In *Greenhouse Gas Control Technologies 7*; Elsevier: Amsterdam, The Netherlands, 2005; Volume II, pp. 1907–1910.
16. Berguerand, N.; Lyngfelt, A. Design and operation of a 10kWth chemical-looping combustor for solid fuels—Testing with South African coal. *Fuel* **2008**, *87*, 2713–2726.
17. Berguerand, N.; Lyngfelt, A. The use of petroleum coke as fuel in a 10kWth chemical-looping combustor. *Int. J. Greenh. Gas Control* **2008**, *2*, 169–179.
18. Shen, L.; Wu, J.; Xiao, J. Chemical-Looping Combustion of Biomass in a 10 kWth Reactor with Iron Oxide As an Oxygen Carrier. *Energy Fuels* **2009**, *23*, 2498–2505.
19. Abdulally, I.; Beal, C.; Andrus, H.; Epple, B.; Lyngfelt, A.; Lani, B. Alstom's chemical looping prototypes, program update. In Proceedings of the 37th International Technical Conference on Clean Coal & Fuel Systems, Clearwater, FL, USA, 31 May–4 June 2012.
20. Ströhle, J.; Orth, M.; Epple, B. Design and operation of a 1 MWth chemical looping plant. *Appl. Energy* **2014**, *113*, 1490–1495.
21. Li, Z. Demonstration of 5 MW chemical looping combustion for solid fuel. In Proceedings of the 14th International Conference on Circulating Fluidized Bed Technology (CFB-14), Taiyuan, China, 21–24 July 2024.

22. Li, Z.; Li, W.; Liu, H.; Duan, Q.; Wang, Y.; Li, J.; Yang, Y.; Cai, N. Development and prospect of chemical looping combustion technology in china. *Proc. CSEE* **2024**, *44*, 7200–7220.
23. Kronberger, B.; Johansson, E.; Löffler, G.; Mattisson, T.; Lyngfelt, A.; Hofbauer, H. A two-compartment fluidized bed reactor for CO_2 capture by chemical-looping combustion. *Chem. Eng. Technol.* **2004**, *27*, 1318–1326.
24. Adánez, J.; Gayán, P.; Celaya, J.; de Diego, L.F.; García-Labiano, F.; Abad, A. Chemical looping combustion in a 10 kWth prototype using a CuO/Al_2O_3 oxygen carrier: Effect of operating conditions on methane combustion. *Ind. Eng. Chem. Res.* **2006**, *45*, 6075–6080.
25. Bolhàr-Nordenkampf, J.; Pröll, T.; Kolbitsch, P.; Hofbauer, H. Performance of a NiO-based oxygen carrier for chemical looping combustion and reforming in a 120 kW unit. *Energy Procedia* **2009**, *1*, 19–25.
26. Lyngfelt, A. Chemical-looping combustion of solid fuels—Status of development. *Appl. Energy* **2014**, *113*, 1869–1873.
27. Lyngfelt, A.; Linderholm, C. Chemical-Looping Combustion of solid fuels—Status and Recent Progress. *Energy Procedia* **2017**, *114*, 371–386.
28. Shen, L.; Wu, J.; Xiao, J. Experiments on chemical looping combustion of coal with a NiO based oxygen carrier. *Combust. Flame* **2009**, *156*, 721–728.
29. Thon, A.; Kramp, M.; Hartge, E.-U.; Heinrich, S.; Werther, J. Operational experience with a system of coupled fluidized beds for chemical looping combustion of solid fuels using ilmenite as oxygen carrier. *Appl. Energy* **2014**, *118*, 309–317.
30. Linderholm, C.; Lyngfelt, A.; Cuadrat, A.; Jerndal, E. Chemical-looping combustion of solid fuels—Operation in a 10kW unit with two fuels, above-bed and in-bed fuel feed and two oxygen carriers, manganese ore and ilmenite. *Fuel* **2012**, *102*, 808–822.
31. Leion, H.; Mattisson, T.; Lyngfelt, A. Solid fuels in chemical-looping combustion. *Int. J. Greenh. Gas Control* **2008**, *2*, 180–193.
32. Bayham, S.; McGiveron, O.; Tong, A.; Chung, E.; Kathe, M.; Wang, D.; Zeng, L.; Fan, L.-S. Parametric and dynamic studies of an iron-based 25-kWth coal direct chemical looping unit using sub-bituminous coal. *Appl. Energy* **2015**, *145*, 354–363.
33. Kim, H.R.; Wang, D.; Zeng, L.; Bayham, S.; Tong, A.; Chung, E.; Kathe, M.V.; Luo, S.; McGiveron, O.; Wang, A.; et al. Coal direct chemical looping combustion process: Design and operation of a 25-kWth sub-pilot unit. *Fuel* **2013**, *108*, 370–384.
34. Mayer, F.; Bidwe, A.R.; Schopf, A.; Taheri, K.; Zieba, M.; Scheffknecht, G. Comparison of a new micaceous iron oxide and ilmenite with respect to syngas conversion in a BFB reactor and adaptation of a 10 kWth DFB system for CLC to solid fuels. In Proceedings of the 2nd International Conference on Chemical Looping, Darmstadt, Germany, 25–27 September 2012.
35. Lighty, J.; Whitty, K.; Smith, P.; Eyring, T. Chemical looping with oxygen uncoupling with coal. In Proceedings of the NETL CO2 Capture Technology Meeting, Pittsburgh, PA, USA, 9–12 July 2012.
36. Thunman, H.; Lind, F.; Breitholtz, C.; Berguerand, N.; Seemann, M. Using an oxygen-carrier as bed material for combustion of biomass in a 12-MWth circulating fluidized-bed boiler. *Fuel* **2013**, *113*, 300–309.
37. Wang, P.; Leion, H.; Yang, H. Oxygen-carrier-aided combustion in a bench-scale fluidized bed. *Energy Fuels* **2017**, *31*, 6463–6471.
38. Garcia, E.; Liu, H. Ilmenite as alternative bed material for the combustion of coal and biomass blends in a fluidised bed combustor to improve combustion performance and reduce agglomeration tendency. *Energy* **2022**, *239*, 121913.
39. Gyllén, A. Oxygen Carrier Aided Combustion: Implementation of Oxygen Carriers to Existing Industrial Settings. Ph.D. Thesis, Chalmers Tekniska Hogskola, Gothenburg, Sweden, 2019.
40. Duan, L.; Li, L. *Oxygen-Carrier-Aided Combustion Technology for Solid-Fuel Conversion in Fluidized Bed*; Springer Nature: Berlin/Heidelberg, Germany, 2023.
41. Moldenhauer, P.; Corcoran, A.; Thunman, H.; Lind, F. A Scale-Up Project for Operating a 115 MWth Biomass-Fired CFB boiler with Oxygen Carriers as Bed Material. In Proceedings of theProceedings of the 5th International Conference on Chemical Looping, Park City, UT, USA, 24–27 September 2018.
42. Zhang, T.; Song, T. Research progress of chemical looping combustion. *Electr. Power Technol. Environ. Prot.* **2024**, *40*, 582–590.
43. Li, Z.; Han, H.; Cai, N. Research status and progress of chemical-looping combustion. *J. Power Eng.* **2006**, *4*, 538–543.
44. Leion, H.; Lyngfelt, A.; Johansson, M.; Jerndal, E.; Mattisson, T. The use of ilmenite as an oxygen carrier in chemical-looping combustion. *Chem. Eng. Res. Des.* **2008**, *86*, 1017–1026.
45. Gu, H.; Shen, L.; Xiao, J.; Zhang, S.; Song, T.; Chen, D. Iron ore as oxygen carrier improved with potassium for chemical looping combustion of anthracite coal. *Combust. Flame* **2012**, *159*, 2480–2490.
46. Gu, H.; Shen, L.; Xiao, J.; Zhang, S.; Song, T. Chemical looping combustion of biomass/coal with natural iron ore as oxygen carrier in a continuous reactor. *Energy Fuels* **2010**, *25*, 446–455.
47. Fraga-Cruz, G.S.; Pérez-Méndez, M.A.; Jiménez-García, G.; Huirache-Acuña, R.; Nápoles-Rivera, F.; Espino-Valencia, J.; Maya-Yescas, R. Integration of Chemical Looping Combustion to a Gasified Stream with Low Hydrogen Content. *Processes* **2024**, *12*, 1033. [CrossRef]
48. Abad, A.; Mattisson, T.; Lyngfelt, A.; Johansson, M. The use of iron oxide as oxygen carrier in a chemical-looping reactor. *Fuel* **2007**, *86*, 1021–1035.
49. Xuan, W.; Zhang, J. Reduction characterization of iron-based oxygen carriers. *J. Eng. Therm. Energy Power*, 2014; 29, 81–85+110–111.

50. Wang, B.; Zhao, H.; Zheng, Y.; Liu, Z.; Yan, R.; Zheng, C. Chemical looping combustion of a Chinese anthracite with Fe_2O_3-based and CuO-based oxygen carriers. *Fuel Process. Technol.* **2012**, *96*, 104–115.
51. Gu, H.M.; Shen, L.H.; Xiao, J.; Zhang, S.W.; Song, T. Cycle experiments on chemical looping combustion of coal using potassium-improved iron ore as oxygen carrier. *J. Fuel Chem. Technol.* **2012**, *40*, 927–934.
52. Chen, D.-Q.; Shen, L.-H.; Xiao, J.; Song, T.; Gu, H.-M.; Zhang, S.-W. Experimental investigation of hematite oxygen carrier decorated with NiO for chemical looping combustion of coal. *J. Fuel Chem. Technol.* **2012**, *40*, 267–272.
53. Bidwe, A.R.; Mayer, F.; Hawthorne, C.; Charitos, A.; Schuster, A.; Scheffknecht, G. Use of ilmenite as an oxygen carrier in chemical looping combustion-batch and continuous dual fluidized bed investigation. *Energy Procedia* **2011**, *4*, 433–440.
54. Cuadrat, A.; Abad, A.; Adánez, J.; de Diego, L.; García-Labiano, F.; Gayán, P. Behavior of ilmenite as oxygen carrier in chemical-looping combustion. *Fuel Process. Technol.* **2012**, *94*, 101–112.
55. Bao, J.; Li, Z.; Sun, H.; Cai, N. Continuous test of ilmenite-based oxygen carriers for chemical looping combustion in a dual fluidized bed reactor system. *Ind. Eng. Chem. Res.* **2013**, *52*, 14817–14827.
56. Cabello, A.; Gayán, P.; García-Labiano, F.; de Diego, L.; Abad, A.; Adánez, J. On the attrition evaluation of oxygen carriers in Chemical Looping Combustion. *Fuel Process. Technol.* **2016**, *148*, 188–197.
57. Li, H.; Sun, Z.; Tian, L.; Gao, L.; Xu, Y.; Cao, Y. The investigation on the attrition of hematite oxygen carrier particles in a fluidization-based chemical looping system. *Fuel Process. Technol.* **2022**, *236*, 107441.
58. Hatanaka, T.; Yoda, Y. Attrition of ilmenite ore during consecutive redox cycles in chemical looping combustion. *Powder Technol.* **2019**, *356*, 974–979.
59. Nelson, T.; van der Watt, J.G.; Laudal, D.; Feilen, H.; Mann, M.; Srinivasachar, S. Reactive jet and cyclonic attrition analysis of ilmenite in chemical looping combustion systems. *Int. J. Greenh. Gas Control* **2019**, *91*, 102837.
60. Shen, T.; Qin, C.; Song, T.; Sun, D. Periodic abrasion and agglomeration development in hematite and ilmenite oxygen carriers: Long-Term redox cycling analysis via fluidized bed TGA. *Fuel* **2025**, *381*, 133400.
61. Bao, J.; Li, Z.; Cai, N. Reduction kinetics of foreign-ion-promoted ilmenite using carbon monoxide (CO) for chemical looping combustion. *Ind. Eng. Chem. Res.* **2013**, *52*, 10646–10655.
62. Ei-Geassy, A.A.; Shehata, K.A.; Ezz, S.Y. Mechanism of iron oxide reduction with hydrogen/carbon monoxide mixtures. *Trans. Iron Steel Inst. Jpn.* **1977**, *17*, 629–635.
63. Et-Tabirou, M.; Dupré, B.; Gleitzer, C. Hematite single crystal reduction into magnetite with CO-CO_2. *Metall. Trans. B* **1988**, *19*, 311–317.
64. Wang, B.; Lv, H.; Zhao, H.; Zheng, C. Experimental and Simulated Investigation of Chemical Looping Combustion of Coal with Fe2O3 based Oxygen Carrier. *Procedia Eng.* **2011**, *16*, 390–395.
65. Monazam, E.R.; Breault, R.W.; Siriwardane, R. Reduction of hematite (Fe_2O_3) to wüstite (FeO) by carbon monoxide (CO) for chemical looping combustion. *Chem. Eng. J.* **2014**, *242*, 204–210.
66. Chen, H.; Zheng, Z.; Shi, W. Investigation on the Kinetics of iron ore fines reduction by CO in a micro-fluidized bed. *Procedia Eng.* **2015**, *102*, 1726–1735.
67. Zhang, Z.; Yao, J.G.; Boot-Handford, M.E.; Fennell, P.S. Pressurised chemical-looping combustion of an iron-based oxygen carrier: Reduction kinetic measurements and modelling. *Fuel Process. Technol.* **2018**, *171*, 205–214.
68. García-Labiano, F.; de Diego, L.F.; Adánez, J.; Abad, A.; Gayán, P. Reduction and oxidation kinetics of a copper-based oxygen carrier prepared by impregnation for chemical-looping combustion. *Ind. Eng. Chem. Res.* **2004**, *43*, 8168–8177.
69. Abad, A.; García-Labiano, F.; de Diego, L.F.; Gayán, P.; Adánez, J. Reduction kinetics of Cu-, Ni-, and Fe-based oxygen carriers using syngas (CO + H_2) for chemical-looping combustion. *Energy Fuels* **2007**, *21*, 1843–1853.
70. Su, M.; Zhao, H.; Tian, X.; Zhang, P.; Du, B.; Liu, Z. Intrinsic reduction kinetics investigation on a hematite oxygen carrier by CO in chemical looping combustion. *Energy Fuels* **2017**, *31*, 3010–3018.
71. Abad, A.; Adánez, J.; García-Labiano, F.; de Diego, L.F.; Gayán, P.; Celaya, J. Mapping of the range of operational conditions for Cu-, Fe-, and Ni-based oxygen carriers in chemical-looping combustion. *Chem. Eng. Sci.* **2007**, *62*, 533–549.
72. Zafar, Q.; Abad, A.; Mattisson, T.; Gevert, B.; Strand, M. Reduction and oxidation kinetics of Mn_3O_4/Mg–ZrO_2 oxygen carrier particles for chemical-looping combustion. *Chem. Eng. Sci.* **2007**, *62*, 6556–6567.
73. Abad, A.; Adánez, J.; García-Labiano, F.; de Diego, L.F.; Gayán, P. Modeling of the chemical-looping combustion of methane using a Cu-based oxygen-carrier. *Combust. Flame* **2010**, *157*, 602–615.
74. Abad, A.; Adánez, J.; Cuadrat, A.; García-Labiano, F.; Gayán, P.; de Diego, L.F. Kinetics of redox reactions of ilmenite for chemical-looping combustion. *Chem. Eng. Sci.* **2011**, *66*, 689–702.
75. Li, Z.; Cai, N. Rate equation theory for gas-solid reaction kinetics. *J. Tsinghua Univ. Sci. Technol.* **2022**, *62*, 704–721.
76. Lee, D. An apparent kinetic model for the carbonation of calcium oxide by carbon dioxide. *Chem. Eng. J.* **2004**, *100*, 71–77.
77. García-Labiano, F.; de Diego, L.F.; Adánez, J.; Abad, A.; Gayán, P. Temperature variations in the oxygen carrier particles during their reduction and oxidation in a chemical-looping combustion system. *Chem. Eng. Sci.* **2005**, *60*, 851–862.

78. Habermann, A.; Winter, F.; Hofbauer, H.; Zirngast, J.; Schenk, J.L. An experimental study on the kinetics of fluidized bed iron ore reduction. *ISIJ Int.* **2000**, *40*, 935–942.
79. Zhu, Q. Chemical-Looping Gasification of Sludge/Coal with Iron-Based Oxygen Carrier. Master's Thesis, Ning Xia University, Ningxia, China, 2021.
80. Mei, D. Experimental and Kinetics Investigation of Iron/Copper/Manganese Based Oxygen Carrier for Chemical Looping Combustion of Coal. Ph.D. Thesis, Huazhong University of Science and Technology, Hubei, China, 2015.
81. Mei, D.; Zhao, H.; Yan, S. Kinetics model for the reduction of Fe_2O_3/Al_2O_3 by CO in Chemical Looping Combustion. *Chem. Eng. Process. Process Intensif.* **2018**, *124*, 137–146.
82. Ksepko, E.; Sciazko, M.; Babinski, P. Studies on the redox reaction kinetics of Fe_2O_3–CuO/Al_2O_3 and Fe_2O_3/TiO_2 oxygen carriers. *Appl. Energy* **2014**, *115*, 374–383.
83. Monazam, E.R.; Breault, R.W.; Siriwardane, R.; Richards, G.; Carpenter, S. Kinetics of the reduction of hematite (Fe_2O_3) by methane (CH_4) during chemical looping combustion: A global mechanism. *Chem. Eng. J.* **2013**, *232*, 478–487.
84. Su, M.; Ma, J.; Tian, X.; Zhao, H. Reduction kinetics of hematite as oxygen carrier in chemical looping combustion. *Fuel Process. Technol.* **2017**, *155*, 160–167.
85. Piotrowski, K.; Mondal, K.; Lorethova, H.; Stonawski, L.; Szymanski, T.; Wiltowski, T. Effect of gas composition on the kinetics of iron oxide reduction in a hydrogen production process. *Int. J. Hydrogen Energy* **2005**, *30*, 1543–1554.
86. Piotrowski, K.; Mondal, K.; Wiltowski, T.; Dydo, P.; Rizeg, G. Topochemical approach of kinetics of the reduction of hematite to wüstite. *Chem. Eng. J.* **2007**, *131*, 73–82.
87. Li, Z.; Sun, H.; Cai, N. Rate Equation Theory for the Carbonation Reaction of CaO with CO_2. *Energy Fuels* **2012**, *26*, 4607–4616.
88. Li, Z. General rate equation theory for gas–solid reaction kinetics and its application to CaO carbonation. *Chem. Eng. Sci.* **2020**, *227*, 115902.
89. Li, Z. First-principles-based microkinetic rate equation theory for oxygen carrier reduction in chemical looping. *Chem. Eng. Sci.* **2022**, *247*, 117042.
90. Li, Z.; Cai, J.; Liu, L. A First-principles microkinetic rate equation theory for heterogeneous reactions: Application to reduction of Fe2O3 in chemical looping. *Ind. Eng. Chem. Res.* **2021**, *60*, 15514–15524.
91. Wang, X.; Chen, Z.; Hu, M.; Tian, Y.; Jin, X.; Ma, S.; Xu, T.; Hu, Z.; Liu, S.; Guo, D.; et al. Chemical looping combustion of biomass using metal ferrites as oxygen carriers. *Chem. Eng. J.* **2017**, *312*, 252–262.
92. Bao, J.; Li, Z.; Cai, N. Promoting the reduction reactivity of ilmenite by introducing foreign ions in chemical looping combustion. *Ind. Eng. Chem. Res.* **2013**, *52*, 6119–6128.
93. Zhou, Z.; Deng, G.; Li, L.; Liu, X.; Sun, Z.; Duan, L. Chemical looping co-conversion of CH_4 and CO_2 using Fe_2O_3/Al_2O_3 pellets as both oxygen carrier and catalyst in a fluidized bed reactor. *Chem. Eng. J.* **2022**, *428*, 132133.
94. Shen, T.; Shen, L. Review of application of FB-TGA in chemical looping combustion reaction kinetics. *J. Huazhong Univ. Sci. Technol. Nat. Sci. Ed.* **2023**, *51*, 133–145.
95. Li, Y.; Li, Z.; Liu, L.; Cai, N. Measuring the fast oxidation kinetics of a manganese oxygen carrier using microfluidized bed thermogravimetric analysis. *Chem. Eng. J.* **2020**, *385*, 123970.
96. Wang, X. Experimental and Modeling Investigation of Coal-Fired Chemical-Looping Combustion Based on the High-Flux Circulating Fluidized Bed Technology. Master's Thesis, Southeast University, Nanjing, China, 2017.
97. Zhu, Q. Study on Oxygen Release Performance and Microscopic Mechanism of Iron—Based Oxygen Carrier. Master's Thesis, China University of Mining and Technology, Xuzhou, China, 2021.
98. Zhao, X.; Bu, C.; Wang, X.; Zhang, X.; Cheng, X.; Wang, N.; Piao, G. Kinetics investigation on iron-based oxygen carrier aided oxy-fuel combustion of anthracite char. *CIESC J.* **2022**, *73*, 384–392.
99. Liu, H. The Performance Research on Reaction of Fe-Based Oxygen Carrier and CO in Chemical-Looping Combustion Process. Master's Thesis, North China Electric Power University, Beijing, China, 2012.
100. Liu, F.; Zhang, Y.; Chen, L.; Qian, D.; Neathery, J.K.; Kozo, S.; Liu, K. Investigation of a canadian ilmenite as an oxygen carrier for chemical looping combustion. *Energy Fuels* **2013**, *27*, 5987–5995.
101. Ksepko, E.; Babiński, P.; Nalbandian, L. The redox reaction kinetics of Sinai ore for chemical looping combustion applications. *Appl. Energy* **2017**, *190*, 1258–1274.
102. Steiner, T.; Schulze, K.; Kienzl, N.; Pauritsch, M.; Hacker, V.; Bock, S.; Abad, A.; Scharler, R.; Anca-Couce, A. Chemical looping of synthetic ilmenite, Part I: Addressing challenges of kinetic TGA measurements with H_2. *Fuel* **2024**, *368*, 131528.
103. Khakpoor, N.; Mostafavi, E.; Mahinpey, N.; De la Hoz Siegler, H. Oxygen transport capacity and kinetic study of ilmenite ores for methane chemical-looping combustion. *Energy* **2019**, *169*, 329–337.
104. Dilmaç, N. Isothermal and non-isothermal reduction kinetics of iron ore oxygen carrier by CO: Modelistic and model-free approaches. *Fuel* **2021**, *296*, 120707.
105. Luo, M.; Wang, S.; Wang, L.; Lv, M. Reduction kinetics of iron-based oxygen carriers using methane for chemical-looping combustion. *J. Power Sources* **2014**, *270*, 434–440.

106. Mendiara, T.; Abad, A.; de Diego, L.F.; García-Labiano, F.; Gayán, P.; Adánez, J. Reduction and oxidation kinetics of Tierga iron ore for chemical looping combustion with diverse fuels. *Chem. Eng. J.* **2019**, *359*, 37–46.
107. Nasr, S.; Plucknett, K.P. Kinetics of iron ore reduction by methane for chemical looping combustion. *Energy Fuels* **2014**, *28*, 1387–1395.
108. Cabello, A.; Abad, A.; García-Labiano, F.; Gayán, P.; de Diego, L.F.; Adánez, J. Kinetic determination of a highly reactive impregnated Fe_2O_3/Al_2O_3 oxygen carrier for use in gas-fueled Chemical Looping Combustion. *Chem. Eng. J.* **2014**, *258*, 265–280.
109. Li, Y.; Wang, Y.; Liu, K.; Zhao, H. Reduction Kinetics of Low-Cost Cu/Fe-Based Oxygen Carriers in Chemical Looping Mode. *Energy Fuels* **2023**, *37*, 16716–16728.
110. Moed, N.M.; Chiang, M.-H.; Ku, Y.; Tseng, Y.-H. Kinetics for chemical looping process with fabricated Fe_2O_3-CuO/Al_2O_3 oxygen carriers. *Chem. Eng. Sci.* **2022**, *258*, 117730.
111. Li, Q.; Qin, W.; Zhang, J.-J.; Cheng, W.-L.; Dong, C.-Q. Characteristics and kinetics of chemical looping combustion of Mn-doped Fe2O3 oxygen carrier with CO. *J. Fuel Chem. Technol.* **2014**, *42*, 932–937.
112. Wang, Y.D.; Hua, X.N.; Zhao, C.C.; Fu, T.T.; Li, W.; Wang, W. Step-wise reduction kinetics of Fe_2O_3 by CO/CO_2 mixtures for chemical looping hydrogen generation. *Int. J. Hydrogen Energy* **2017**, *42*, 5667–5675.
113. Choisez, L.; Hemke, K.; Özgün, Ö.; Pistidda, C.; Jeppesen, H.; Raabe, D.; Ma, Y. Hydrogen-based direct reduction of combusted iron powder: Deep pre-oxidation, reduction kinetics and microstructural analysis. *Acta Mater.* **2024**, *268*, 119752.
114. Chai, Y.; Zhang, J.; Zhang, X.; Zhang, Z.; Luo, G.; An, S.; Bu, E. Non-isothermal kinetic study of pure-hydrogen reduction for various iron-containing raw materials. *Int. J. Hydrogen Energy* **2024**, *81*, 707–717.
115. Abdel Halim, K.S.; Khedr, M.H.; Soliman, N.K. Reduction characteristics of iron oxide in nanoscale. *Mater. Sci. Technol.* **2010**, *26*, 445–452.
116. Alonso, M.; Criado, Y.A.; Abanades, J.C.; Grasa, G. Undesired effects in the determination of CO_2 carrying capacities of CaO during TG testing. *Fuel* **2014**, *127*, 52–61.
117. Stanmore, B.; Gilot, P.; Prado, G. The influence of mass transfer in DTG combustion tests. *Thermochim. Acta* **1994**, *240*, 79–89.
118. Cardona, M.; Boffito, D.C.; Patience, G.S. Thermogravimetric heat and mass transfer: Modeling of bitumen pyrolysis. *Fuel* **2015**, *143*, 253–261.
119. Wu, L. Experimental Investigation on Reduction Reaction Kinetics and Hydrogen Generation Process of Iron Ore as Oxygen Carrier. Master's Thesis, Southeast University, Nanjing, China, 2017.
120. Schwebel, G.L.; Sundqvist, S.; Krumm, W.; Leion, H. Apparent kinetics derived from fluidized bed experiments for Norwegian ilmenite as oxygen carrier. *J. Environ. Chem. Eng.* **2014**, *2*, 1131–1141. [CrossRef]
121. Perreault, P.; Patience, G.-S. Ilmenite–CO reduction kinetics. *Fuel* **2016**, *165*, 166–172.
122. Yu, J.-W.; Han, Y.-X.; Gao, P.; Li, Y.-J. Reductive Transformation of Hematite to Magnetite with CO/CO_2 under fluidized bed conditions. *J. Northeast. Univ. Nat. Sci.* **2019**, *40*, 261–266.
123. Zhang, Z.; Hills, T.P.; Scott, S.A.; Fennell, P.S. Spouted bed reactor for kinetic measurements of reduction of Fe_2O_3 in a CO_2/CO atmosphere Part I: Atmospheric pressure measurements and equipment commissioning. *Chem. Eng. Res. Des.* **2016**, *114*, 307–320.
124. Alsabak, B.M.J.; Dilmaç, N. Ferronickel production via selective reduction of turkish laterite ore by h2 in fluidized bed reactor: Isothermal kinetic modeling. *Metall. Mater. Trans. B* **2024**, *56*, 33–45.
125. Spreitzer, D.; Schenk, J. Iron ore reduction by hydrogen using a laboratory scale fluidized bed reactor: Kinetic investigation—Experimental setup and method for determination. *Metall. Mater. Trans. B* **2019**, *50*, 2471–2484.
126. Purnomo, V.; Mei, D.; Staničić, I.; Mattisson, T.; Leion, H. Effect of the conversion degree on the apparent kinetics of iron-based oxygen carriers. *Energy Fuels* **2024**, *38*, 11824–11836.
127. Chiron, F.-X.; Patience, G.S. Kinetics of mixed copper–iron based oxygen carriers for hydrogen production by chemical looping water splitting. *Int. J. Hydrogen Energy* **2012**, *37*, 10526–10538.
128. Cheng, Y.; Liu, Y.; Tian, H.; Guo, Q. Chemical-looping gasification reaction characteristics and mechanism of coal and Fe-based composite oxygen carriers. *CIESC J.* **2013**, *64*, 2587–2595.
129. Feilmayr, C.; Thurnhofer, A.; Winter, F.; Mali, H.; Schenk, J. reduction behavior of hematite to magnetite under fluidized bed conditions. *ISIJ Int.* **2004**, *44*, 1125–1133.
130. Narindri Rara Winayu, B.; Li, J.-D.; Chu, H. Fe-based oxygen carrier for the chemical looping combustion of CO, H_2, and CH_4 syngas in fluidized bed reactor under interruption of H_2S. *Chem. Eng. Res. Des.* **2023**, *194*, 514–528.
131. Narindri Rara Winayu, B.; Li, C.-T.; Chu, H. Effective performance of ilmenite oxygen carrier for chemical looping combustion of carbon monoxide, hydrogen, and methane in a fluidized bed reactor. *J. Clean. Prod.* **2022**, *379*, 134881.
132. Chen, H.; Zheng, Z.; Chen, Z.; Bi, X.T. Reduction of hematite (Fe_2O_3) to metallic iron (Fe) by CO in a micro fluidized bed reaction analyzer: A multistep kinetics study. *Powder Technol.* **2017**, *316*, 410–420.
133. Zeng, D.; Li, Y.; Zhang, Z.; Luo, C.; Liu, T.; Kong, Q.; Xiao, R. Bulk oxygen conduction kinetics of iron oxides on the chemical looping combustion. *Fuel Process. Technol.* **2022**, *237*, 107442.
134. Liu, X.; Zhang, H.; Hong, H. Reduction kinetics of fe-based oxygen carriers using syngas in a honeycomb fixed-bed reactor for chemical-looping combustion. *J. Therm. Sci.* **2019**, *29*, 13–24.

135. Fennell, P.S.; Kadchha, S.; Lee, H.Y.; Dennis, J.S.; Hayhurst, A.N. The measurement of the rate of burning of different coal chars in an electrically heated fluidised bed of sand. *Chem. Eng. Sci.* **2007**, *62*, 608–618.
136. Latifi, M.; Chaouki, J. A novel induction heating fluidized bed reactor: Its design and applications in high temperature screening tests with solid feedstocks and prediction of defluidization state. *AIChE J.* **2015**, *61*, 1507–1523.
137. Samih, S.; Chaouki, J. Development of a fluidized bed thermogravimetric analyzer. *AIChE J.* **2014**, *61*, 84–89.
138. Saadatkhah, N.; Carillo Garcia, A.; Ackermann, S.; Leclerc, P.; Latifi, M.; Samih, S.; Patience, G.S.; Chaouki, J. Experimental methods in chemical engineering: Thermogravimetric analysis—TGA. *Can. J. Chem. Eng.* **2019**, *98*, 34–43.
139. Liu, L.; Li, Z.; Li, Z.; Larring, Y.; Li, Y.; Cai, N. Fast redox kinetics of a perovskite oxygen carrier measured using micro-fluidized bed thermogravimetric analysis. *Proc. Combust. Inst.* **2021**, *38*, 5259–5269.
140. Li, Y.; Wang, H.; Li, W.; Li, Z.; Cai, N. CO2 gasification of a lignite char in microfluidized bed thermogravimetric analysis for chemical looping combustion and chemical looping with oxygen uncoupling. *Energy Fuels* **2018**, *33*, 449–459.
141. Shen, T.; Yan, J.; Zhu, X.; Wang, L.; Shen, L. Catalytic combustion behaviors of petroleum coke with hematite catalyst in a micro fluidized bed thermogravimetric analysis. *Chem. Eng. J.* **2021**, *422*, 130087.
142. Yan, J.; Shen, T.; Wang, P.; Yin, X.; Zhu, X.; Jiang, S.; Shen, L. Redox performance of manganese ore in a fluidized bed thermogravimetric analyzer for chemical looping combustion. *Fuel* **2021**, *295*, 120564.
143. Liu, L.; Li, Z.; Li, Z.; Larring, Y.; Cai, N. Heterogeneous reaction kinetics of a perovskite oxygen carrier for chemical looping combustion coupled with oxygen uncoupling. *Chem. Eng. J.* **2021**, *417*, 128054.
144. Wang, Y.; Li, Z.; Cai, N. Redox reaction kinetics of a Fe–Cu-based oxygen carrier measured with microfluidized bed thermogravimetric analysis. *Energy Fuels* **2022**, *36*, 9672–9686.
145. Shen, T.; Shen, L.; Song, T. Multiscale gas–solid reaction dynamics of hematite oxygen carrier in chemical looping combustion from fluidized bed thermogravimetric analysis. *Energy Fuels* **2024**, *38*, 8909–8927.
146. Liu, X.; Li, Z.; Shen, L.; Ma, J.; Liu, X.; He, D.; Zhao, H. Quantitative evaluation of four oxygen carriers for natural gas chemical looping combustion. *Proc. Combust. Inst.* **2024**, *40*, 105641.
147. Ma, J.; Tian, X.; Wang, C.; Chen, X.; Zhao, H. Performance of a 50 kWth coal-fuelled chemical looping combustor. *Int. J. Greenh. Gas Control* **2018**, *75*, 98–106.
148. Huang, Z.; He, F.; Feng, Y.; Zhao, K.; Zheng, A.; Chang, S.; Li, H. Synthesis gas production through biomass direct chemical looping conversion with natural hematite as an oxygen carrier. *Bioresour. Technol.* **2013**, *140*, 138–145.
149. Ge, H.; Guo, W.; Shen, L.; Song, T.; Xiao, J. Experimental investigation on biomass gasification using chemical looping in a batch reactor and a continuous dual reactor. *Chem. Eng. J.* **2016**, *286*, 689–700.
150. Ge, H.; Guo, W.; Shen, L.; Song, T.; Xiao, J. Biomass gasification using chemical looping in a 25 kW th reactor with natural hematite as oxygen carrier. *Chem. Eng. J.* **2016**, *286*, 174–183.
151. Liu, W.; Lim, J.Y.; Saucedo, M.A.; Hayhurst, A.N.; Scott, S.A.; Dennis, J.S. Kinetics of the reduction of wüstite by hydrogen and carbon monoxide for the chemical looping production of hydrogen. *Chem. Eng. Sci.* **2014**, *120*, 149–166.
152. Khani, M.; Ale Ebrahim, H.; Habibzadeh, S. A comprehensive random pore model kinetic study of hematite to iron reduction by hydrogen. *Chem. Eng. Sci.* **2023**, *281*, 119116.
153. Yang, W.; Zhao, H.; Wang, K.; Zheng, C. Synergistic effects of mixtures of iron ores and copper ores as oxygen carriers in chemical-looping combustion. *Proc. Combust. Inst.* **2015**, *35*, 2811–2818.
154. Rydén, M.; Johansson, M.; Cleverstam, E.; Lyngfelt, A.; Mattisson, T. Ilmenite with addition of NiO as oxygen carrier for chemical-looping combustion. *Fuel* **2010**, *89*, 3523–3533.
155. Mattisson, T.; Johansson, M.; Lyngfelt, A. Multicycle reduction and oxidation of different types of iron oxide particlesapplication to chemical-looping combustion. *Energy Fuels* **2004**, *18*, 628–637.
156. Yang, W.; Zhao, H.; Ma, J.; Mei, D.; Zheng, C. Copper-decorated hematite as an oxygen carrier for in situ gasification chemical looping combustion of coal. *Energy Fuels* **2014**, *28*, 3970–3981.
157. Jiang, S.; Shen, L.; Wu, J.; Yan, J.; Song, T. The investigations of hematite-CuO oxygen carrier in chemical looping combustion. *Chem. Eng. J.* **2017**, *317*, 132–142.
158. Bao, J.; Liu, W.; Cleeton, J.P.E.; Scott, S.A.; Dennis, J.S.; Li, Z.; Cai, N. Interaction between Fe-based oxygen carriers and n-heptane during chemical looping combustion. *Proc. Combust. Inst.* **2013**, *34*, 2839–2846.
159. Siriwardane, R.; Tian, H.; Simonyi, T.; Poston, J. Synergetic effects of mixed copper–iron oxides oxygen carriers in chemical looping combustion. *Fuel* **2013**, *108*, 319–333.
160. Jin, B.; Fan, Y.; Lv, Y.; Li, G.; Zhao, H.; Liang, Z. Low concentration Ni doping to intensify redox kinetics of iron-based oxygen carriers for efficient chemical looping reverse water gas shift. *Sep. Purif. Technol.* **2025**, *360*, 131237.
161. Li, Y.; Liu, M.; Liu, Y.; Shen, Y.; Pan, Y.; Jin, H. Reaction kinetics of Ni-Fe oxygen carriers with high performance for chemical looping hydrogen production. *Chem. Eng. J.* **2024**, *499*, 156067.
162. Su, M.; Zhao, H.; Du, B.; Zhang, P.; Liu, Z. Experimental investigation for the intrinsic reduction kinetics of a hematite as oxygen carrier in chemical looping combustion. *Shandong Sci.* **2017**, *30*, 41–51.

163. Bohn, C.D.; Cleeton, J.P.; Müller, C.R.; Davidson, J.F.; Hayhurst, A.N.; Scott, S.A.; Dennis, J.S. The kinetics of the reduction of iron oxide by carbon monoxide mixed with carbon dioxide. *AIChE J.* **2009**, *56*, 1016–1029.
164. Pineau, A.; Kanari, N.; Gaballah, I. Kinetics of reduction of iron oxides by H2. *Thermochim. Acta* **2006**, *447*, 89–100.
165. Siriwardane, R.; Tian, H.; Richards, G.; Simonyi, T.; Poston, J. Chemical-looping combustion of coal with metal oxide oxygen carriers. *Energy Fuels* **2009**, *23*, 3885–3892.
166. Xiao, R.; Song, Q.; Song, M.; Lu, Z.; Zhang, S.; Shen, L. Pressurized chemical-looping combustion of coal with an iron ore-based oxygen carrier. *Combust. Flame* **2010**, *157*, 1140–1153.
167. Bao, J.; Li, Z.; Cai, N. Interaction between iron-based oxygen carrier and four coal ashes during chemical looping combustion. *Appl. Energy* **2014**, *115*, 549–558.
168. Rubel, A.; Zhang, Y.; Neathery, J.K.; Liu, K. Comparative study of the effect of different coal fly ashes on the performance of oxygen carriers for chemical looping combustion. *Energy Fuels* **2012**, *26*, 3156–3161.
169. Azis, M.M.; Leion, H.; Jerndal, E.; Steenari, B.M.; Mattisson, T.; Lyngfelt, A. The effect of bituminous and lignite ash on the performance of ilmenite as oxygen carrier in chemical-looping combustion. *Chem. Eng. Technol.* **2013**, *36*, 1460–1468.
170. Purnomo, V.; Hildor, F.; Knutsson, P.; Leion, H. Interactions between potassium ashes and oxygen carriers based on natural and waste materials at different initial oxidation states. *Greenh. Gases Sci. Technol.* **2023**, *13*, 520–534.
171. Cheng, D.; Yong, Q.; Zhao, Y.; Gong, B.; Zhang, J. Study on the interaction of the Fe-based oxygen carrier with ashes. *Energy Fuels* **2020**, *34*, 9796–9809.
172. Zhou, Y.; Shen, L.; Gu, H.; Niu, X. Effect of biomass ash on performance of iron ore as oxygen carrier in chemical looping combustion. *J. Southeast Univ. Nat. Sci. Ed.* **2015**, *45*, 503–508. [CrossRef]
173. Ilyushechkin, A.Y.; Kochanek, M.; Lim, S. Interactions between oxygen carriers used for chemical looping combustion and ash from brown coals. *Fuel Process. Technol.* **2016**, *147*, 71–82.
174. Yan, J.; Shen, L.; Ou, Z.; Wu, J.; Jiang, S.; Gu, H. Enhancing the performance of iron ore by introducing K and Na ions from biomass ashes in a CLC process. *Energy* **2019**, *167*, 168–180.
175. Gu, H.; Shen, L.; Zhong, Z.; Zhou, Y.; Liu, W.; Niu, X.; Ge, H.; Jiang, S.; Wang, L. Interaction between biomass ash and iron ore oxygen carrier during chemical looping combustion. *Chem. Eng. J.* **2015**, *277*, 70–78.
176. Feng, Y.; Wang, N.; Guo, X. Density functional theory study on improved reactivity of alkali-doped Fe_2O_3 oxygen carriers for chemical looping hydrogen production. *Fuel* **2019**, *236*, 1057–1064.
177. Gu, H.; Shen, L.; Zhong, Z.; Niu, X.; Ge, H.; Zhou, Y.; Xiao, S. Potassium-Modified Iron Ore as Oxygen Carrier for Coal Chemical Looping Combustion: Continuous Test in 1 kW Reactor. *Ind. Eng. Chem. Res.* **2014**, *53*, 13006–13015.
178. Yang, X.; Li, D.; Zhu, X.; Zhu, T.; Mun, T.-Y.; Wang, H.; Bao, G.; Shao, M.; Wang, X. Interaction of ilmenite oxygen carrier with wheat straw ash during chemical looping combustion: Mechanisms and performance variation. *Fuel* **2024**, *374*, 132434.
179. Zhang, Z.; Wang, Y.; Zhu, L.; Li, J.; Wang, F.; Yu, G. Effects of coal ash on iron-based oxygen carrier in chemical-looping combustion using three different rank coals as fuel. *Asia Pac. J. Chem. Eng.* **2019**, *14*, e2313.
180. Guo, X.; Li, Y.; Zhu, Q.; Hu, X.; Ma, J.; Guo, Q. Reactivity of iron-based oxygen carriers with coal ash in pressurized chemical looping gasification. *Fuel Process. Technol.* **2021**, *219*, 106890.
181. Wang, K.; An, Z.; Wang, F.; Liang, W.; Wang, C.; Guo, Q.; Liu, Y.; Yue, G. Effect of ash on the performance of iron-based oxygen carrier in the chemical looping gasification of municipal sludge. *Energy* **2021**, *231*, 120939.
182. Yilmaz, D.; Leion, H. Interaction of iron oxygen carriers and alkaline salts present in biomass-derived ash. *Energy Fuels* **2020**, *34*, 11143–11153.
183. Yilmaz, D.; Steenari, B.-M.; Leion, H. Comparative study: Impacts of ca and mg salts on iron oxygen carriers in chemical looping combustion of biomass. *ACS Omega* **2021**, *6*, 16649–16660. [PubMed]

Disclaimer/Publisher's Note: The statements, opinions and data contained in all publications are solely those of the individual author(s) and contributor(s) and not of MDPI and/or the editor(s). MDPI and/or the editor(s) disclaim responsibility for any injury to people or property resulting from any ideas, methods, instructions or products referred to in the content.